Multi-Proxy Reconstruction of Indian Summer Monsoon Winds and Precipitation of the past 10,000 Years using Mg/Ca and Alkenone Records

Emily C. Gill,[1,2] Balaji Rajagopalan[1,2], Peter H. Molnar[2,3], Yochanan Kushnir[4], and Thomas M. Marchitto[3,5]

Corresponding author: Emily Gill, Cooperative Institute of Research in Environmental Science (CIRES), University of Colorado at Boulder, Campus Box 216, Boulder, Colorado 80309-0216, USA. (emily.gill@colorado.edu)

[1]Department of Civil, Environmental and

Using a multi-proxy reduced dimension methodology we reconstruct full fields of summer wind stress curl and rainfall anomalies over the Indian monsoon region since the early-Holocene using SST proxies (Mg/Ca and alkenones) from forty locations scattered across the Arabian Sea, the Bay of Bengal, and the east and west equatorial Pacific. Reconstructions of summer wind stress curl reveal that the greatest magnitudes of positive wind stress curl, $\sim 30\%$ greater than present day, off the coastlines of Oman and Yemen occurred at

Architectural Engineering, University of Colorado at Boulder, Boulder, CO, USA.

[2]Cooperative Institute for Research in Environmental Sciences (CIRES), Boulder, CO, USA.

[3]Department of Geological Sciences, University of Colorado at Boulder, Boulder, CO, USA.

[4]Lamont-Doherty Earth Observatory (LDEO), Columbia University, Palisades, NY, USA.

[5]Institute of Arctic and Alpine Research (INSTARR), University of Colorado at Boulder, Boulder, CO, USA.

10 ka, suggesting enhanced ocean upwelling and a strong monsoon jet during this time. Strong positive anomalies in these regions continued but weakened slightly from 8 to 6 ka, and by 2 to 4 ka, to 10-20% greater than present day. This pattern is consistent with studies that used the fraction of *Globigerina bulloides* to reconstruct upwelling strength in the western Arabian Sea over the past 10 ka. Spatial rainfall reconstructions reveal the greatest difference in precipitation at 10 ka over the core monsoon region (20-60% greater than present day), and concurrently the greatest deficit in rainfall in North East India and on the eastern side of the Western Ghats (10-30% less than present day). Rainfall over the core monsoon region was about 30% greater than present day from 8 to 6 ka, but decreased to not much more than 20% greater from 4 to 2 ka. These findings advance the hypothesis that teleconnections from the equatorial Pacific could account for greater early- to mid-Holocene wetness over India as recorded by various paleoclimate proxies.

1. Introduction

Paleoclimatic evidence from climate proxy data suggests that India has aridified over the past 10 thousand years (ka) (Figure 1). The predominantly cited explanation rests on the idea that greater summer insolation in early Holocene time, due to the precessional cycle, caused greater heating of the Indian subcontinent, which increased the land-ocean temperature gradient and created a stronger early than late Holocene monsoon [e.g. *Kutzbach*, 1981; *Kutzbach and Otto-Bliesner*, 1982; *Liu et al.*, 2000]. This idea relies on the traditional understanding of monsoon dynamics. The monsoon begins each year in mid-May due to the intense spring heating of the Indian subcontinent and possibly the Tibetan Plateau, which creates a temperature, and thus, surface pressure gradient between the land and the surrounding ocean that forces the monsoon jet [e.g. *Li and Yanai*, 1996; *Wu et al.*, 2007], at least during the early (mid-May to mid-June) and late (Sep to mid-Oct) seasons [*Rajagopalan and Molnar*, 2013]. In principle, over the course of the entire monsoon season, the degree of the local land warming can modulate the strength not only of the monsoon jet but also of rainfall. Therefore, a sensible hypothesis follows that enhanced land warming during the early- to mid-Holocene contributed to greater wetness over India. Since the mid-1990s, however, surface temperatures over India have risen dramatically while monsoon rainfall has remained below average [*Krishna Kumar et al.*, 2011], which suggests that other processes also affect monsoon strength, whether measured by rainfall or wind speeds.

Teleconnections from the equatorial Pacific phenomena - El Niño-Southern Oscillation (ENSO) - also modulate the strength of the monsoon on inter-annual time scales. During

La Niña (El Niño), when central and eastern tropical Pacific SSTs are anomalously cool (warm), monsoon rainfall commonly is strong (weak). There is an asymmetry in this relationship [*Krishna Kumar et al.*, 2006] in that La Niña conditions almost always are associated with high monsoon rainfall, but El Niño conditions have historically resulted in either normal or weak rainfall. *Krishna Kumar et al.* [2006] attribute this asymmetry to the location of El Niño-related warming in the Pacific and suggest that central Pacific warming favors drought more than eastern Pacific warming.

Proxy records from the east and west Pacific that reconstruct SSTs throughout the past 10 ka suggest a shift from a more La Niña-like state during the early- to mid-Holocene to a more El Niño-like state during the late-Holocene [e.g. *Conroy et al.*, 2008; *Koutavas et al.*, 2002, 2006; *Leduc et al.*, 2007, 2010; *Pahnke et al.*, 2007; *Stott et al.*, 2002, 2004]. Additionally, primary productivity records from the Banda Sea [*Beaufort et al.*, 2010] and sediment records from lakes in Ecuador and Peru [e.g. *Chazen et al.*, 2009; *Moy et al.*, 2002; *Riedinger et al.*, 2002; *Rein et al.*, 2005; *Rodbell et al.*, 1999; *Sandweiss et al.*, 1996, 2001] suggest that ENSO variability increased after the mid-Holocene. Climate model simulations for Holocene time also suggest a cooler equatorial Pacific and rare El Niño events until around 6 ka [e.g. *Clement et al.*, 1999, 2000; *Emile-Geay et al.*, 2007].

Assuming the contemporary relationship between ENSO and the monsoon persisted through the past 10 ka, and given the consistent correlation of La Niña with strong monsoon rainfall, we advance a second hypothesis that is independent of land-warming over India: equatorial Pacific cooling (i.e. La Niña-like state) during the early to mid-Holocene contributed to greater rainfall over India. Following similar logic, the return of

ENSO variability during the late Holocene could have contributed to aridification in late Holocene. As these two hypotheses (land-warming and ENSO) are not mutually exclusive, we aim not to disprove the land-warming hypothesis, but to test the plausibility of the ENSO hypothesis.

To do so, we exploit SST proxy data from the eastern and western equatorial Pacific (Tables 1 and 2, Figures 1 and 2) and from the Indian Ocean (Table 3, Figure 3). *Gill et al.* [2015, in review] used a reduced-dimension multi-proxy reconstruction approach to combine magnesium/calcium (Mg/Ca) and alkenone ($U^{k'}_{37}$) SST records from the east and west Pacific to reconstruct full fields of tropical Pacific SSTs and zonal winds. We found that the coldest eastern equatorial Pacific SST anomalies occurred during the early Holocene (10 ka), but the largest reconstructed zonal SST differences between east and west Pacific occurred during 10 and 6 ka. The smallest zonal differences were seen from 4 to 2 ka. This timeline is consistent with an enhanced La Niña-like state during the early- to mid-Holocene, but not during the late Holocene.

Motivated by the correlation of rainfall over India with La Niña and the scattered proxy records across the Indian monsoon region in Figure 1 (explained in further detail in the following section), we ask: Could the aridification of India since 10 ka be attributed, at least in part, to teleconnections from the Pacific? We use the same reduced-dimension multi-proxy reconstruction approach [*Gill et al.*, 2015, in review] to reconstruct full fields of summer wind stress curl over the Arabian Sea and Indian summer monsoon rainfall anomalies for the past 10 ka using only SST proxy records from the Indo-Pacific region along with contemporary patterns of variability.

2. Paleoclimatic Evidence of a Wetter India

Evidence suggesting a stronger early- to mid-Holocene ($\sim$ 10-6 ka BP) Indian summer monsoon includes both continental and marine proxy records from the monsoonal region of southern Oman across India to the Bay of Bengal (Figure 1). Greater precipitation during the early- to mid-Holocene than late-Holocene (post 4 ka) has been inferred [*Bryson and Swain*, 1981; *Swain et al.*, 1983] from pollen reconstructions [*Singh et al.*, 1972, 1973, 1974, 1990] and lake-bed sediment records [*Achyuthan et al.*, 2007; *Deotare et al.*, 2004; *Enzel et al.*, 1999; *Kajale and Deotare*, 1997; *Prasad et al.*, 1997; *Wasson et al.*, 1984] from northwestern India. Although the lakes Bap Malar, Didwana, Kanod, Lunkaransar, Nal Sarovar, Sambhar, Tal Chapar, and Parihara (Figure 1, blue) did not dry up simultaneously, each shows maximum wetness occurring sometime during the early- to mid-Holocene, followed by a period of aridification during the late Holocene. Interestingly, a carbon isotope record obtained from peat located in Nilgiri Hills region of south India (Figure 1, yellow) shows an arid phase during the mid-Holocene followed by a wetter phase in the recent period [*Sukumar et al.*, 1993]. Though opposite to those cited above for the region to the north, his finding is actually consistent with the lake records, as this region, positioned in the rain shadow of the Western Ghats, is typically out of phase with the rest of the sub-continent in present-day rainfall [e.g. *Gill et al.*, 2015a].

Marine isotope records from boreholes located just south of the mouths of major Indian river systems that empty into the Arabian Sea and Bay of Bengal have also been exploited to reconstruct isotope or sediment records that reflect discharge during the past 10 ka. In the Arabian Sea, *Staubwasser et al.* [2003] used δ^{18}O from the mouth of the Indus

River (Figure 1, 63KA) from the last 6 ka to infer a drastic reduction in discharge at 4.2 ka, which is concurrent with the termination of the ancient Harappan civilization that inhabited the Indus Valley. Farther south, numerous rivers drain from the Western Ghats into the eastern Arabian Sea. Oxygen isotopes from a sediment core just off the coast (Figure 1, red 3268G5) has been used to reconstruct Holocene evaporation minus precipitation, and *Sarkar et al.* [2000] inferred relatively high precipitation from 10 to 6 ka, followed by an arid episode from 3.5 to 2 ka. For the Bay of Bengal, *Ponton et al.* [2012] used a borehole (NGHP-16A) located at about 16°N (Figure 1, red 16A) to reconstruct changes in vegetation in the Godavari River basin as well as salinity changes in the Bay. They report a period of aridity beginning at 4 ka and unprecedented high salinity from 3 ka to present-day, implying lower precipitation and lower river discharge during the late Holocene compared to either the early- or mid-Holocene. Farther north *Kudrass et al.* [2001] used alkenone temperature data [*Sonzogni et al.*, 1998] and δ^{18}O data [*Rostek et al.*, 1993] from SO93-126KL (Figure 1, red 126KL) to reconstruct salinity at the mouth of the Ganges River in the northern Bay of Bengal. They found that salinity decreased during the early Holocene, reaching a minimum at 6 ka, and subsequently increased until present-day. In the same region, *Goodbred and Kuehl* [2000] analyzed over 50 borehole records scattered across the coastal region of Bangladesh (Figure 1, purple box) to reconstruct sediment discharge from the Ganges and found high sediment discharge from 11 to 7 ka. This, combined with the findings of *Kudrass et al.* [2001], suggests that river discharge from the Ganges, which is reflective of precipitation over the Indo-Gangetic Plains, was high during the early- and mid-Holocene.

Monsoon variability and strength has also been reconstructed using continental and marine records from Oman and the western Arabian Sea, where biological productivity and isotope proxies are used to infer ocean upwelling, wind strength, and precipitation for the past 10 ka. Speleothem records in Oman from the Hoti Cave [*Neff et al.*, 2001; *Fleitmann et al.*, 2003, 2007], Qunf Cave [*Fleitmann et al.*, 2003, 2007] and Defore Cave [*Fleitmann et al.*, 2007] suggest a more intense rainfall during early Holocene but decreasing monsoon strength during the mid- to late-Holocene (Figure 1, orange). When the monsoon jet sweeps across the coastlines of Somalia and Oman, it induces upwelling, which enhances biological productivity. *G. bulloides* is a planktic foraminifer that thrives in this cold nutrient-rich upwelling water during the monsoon and acts as a proxy for wind strength [e.g. *Curry et al.*, 1992; *Prell and Curry*, 1981]. A high-resolution record provided by [e.g. *Curry et al.*, 1992; *Prell and Curry*, 1981] from core site ODP-723A reveals a monotonic decrease in *G. bulloides* between 10 and 2 ka, which they inferred to imply decreasing strength of winds during the summer monsoon. Another productivity record (using Ba/Al ratios from *N.dutertrei*) off the Somali coast (NIOP-905) also implies decreased upwelling from 10 ka to present [*Ivanochko et al.*, 2005].

3. Modern Data

Contemporary (1901-2013) gridded (2° by 2°) monthly SSTs were obtained from the NOAA NCDC Extended Reconstruction Sea Surface Temperature (ERSST) version 3b dataset [*Smith et al.*, 2008]. Contemporary monthly gridded (1.875° by 1.875°) wind stress curl (10^{-8} kg m^{-2} s^{-2}) was calculated using NOAA NCEP-NCAR CDAS-1 zonal and meridional momentum flux data for the period 1949-2013 [*Kalnay et al.*, 1996] and

masked to include the surface wind stress curl only over Arabian Sea grid cells. Monthly anomalies were calculated for each dataset using the 1981-2010 climatology. Monthly SST anomalies were then converted to annual averages by averaging from May to the following April in order to capture the annual ENSO cycle. Summer wind stress curl anomalies were calculated by averaging June, July, August and September anomalies. Daily gridded (1° by 1°) rainfall was obtained from the India Meteorological Department [Rajeevan et al., 2006]. Seasonal average daily rainfall (mm d^{-1}) time series were created for each grid point by averaging the daily totals from 1 Jun to 30 Sep over the 1901-2004 period.

Two common paleo-proxy records are used: magnesium/calcium ratios in planktonic foraminifera (Mg/Ca) and an index of unsaturation in alkenones ($U_{37}^{k'}$ that are formed at shallow depths. See *Gill et al.* [2015, in review] for more information on the use of these proxies in this reconstruction framework. *Lea et al.* [1999] and *Nürnberg et al.* [1996] summarize Mg/Ca paleothermometry, and *Brassell et al.* [1986] and *Herbert* [2003] describe $U_{37}^{k'}$ paleothermometry.

There are 43 total SST proxy records (20 Mg/Ca and 23 $U_{37}^{k'}$), but for 3 sites both types of proxy records have been obtained (Tables 1-3). In those instances, we use the Mg/Ca records instead of the $U_{37}^{k'}$ to be consistent with *Gill et al.* [2015, in review]. As shown in Figures 2-4, these records are sampled at various temporal resolutions. We, therefore, smooth the raw SST records using a local polynomial method with a second order polynomial and a local neighborhood consisting of 70% of the nearest data points [e.g. *Loader et al.*, 1996]. These records were then converted to SST anomalies using the climatological mean temperature from ERSST at the grid-cell closest to the

location of the proxy record. All paleo-SST records were obtained from the archives of NCDC (http://www.ncdc.noaa.gov/data-access/paleoclimatology-data/datasets) and Pangaea (http://www.pangaea.de/).

4. Methodology

During the summer season, SSTs over northern Indian Ocean (Arabian Sea and Bay of Bengal) are modulated by the monsoon [*Krishnamurthy and Kirtman*, 2003], wherein strong winds enable cooler SSTs from coastal upwelling and evaporative cooling. Therefore, reconstructing the winds obviates the need for SST reconstructions. Indian Ocean SSTs exhibit a well documented [e.g. *Allan et al.*, 1995; *Terray and Dominiak*, 2005; *Ihara et al.*, 2008; *Roxy et al.*, 2014] recent warming trend largely attributed to anthropogenic sources. This anthropogenic SST signal, which might have been imparted to the wind stress curl, must be removed so that only the non-anthropogenic variability is reconstructed. To this end, first, a principal component analysis (PCA) of 1949-2013 ERSST Indian Ocean SSTs was performed and as expected the first orthogonal mode accounts for nearly 70% of the total variability in the data (Figure 5b), and is characterized by a strong warming trend (Figure 5a). Each of the remaining modes, however, explains only a small fraction of the remaining variance (Figure 5b). Then we regressed summer wind stress curl at each of the 262 grid points over the Arabian Sea against the first Principal Component (PC). The residuals from the regression represent the de-trended wind stress curl time series at each grid point containing the non-anthropogenic variability.

Interannual variability of monsoonal winds and consequently the Indian summer rainfall are influenced by the Walker Circulation, which is directly affected by equatorial Pacific

SSTs [e.g. *Krishna Kumar et al.*, 1995; *Parthasarathy and Pant*, 1985; *Shukla and Mooley*, 1987; *Shukla and Paolino*, 1983; *Webster*, 1987; *Webster et al.*, 1998] and to a lesser extent Indian Ocean SSTs. Therefore, to reconstruct variations in monsoon strength, we use SST proxy records from the Indian Ocean and equatorial Pacific to reconstruct anomalies both in Arabian Sea summer wind stress curl and in monsoon rainfall over India. The reconstruction methodology consists of two key steps on the contemporary fields - (i) using PCA to isolate a small number of leading modes of variability in the contemporary limited SST field (i.e. SSTs at the locations of the proxy data) and the contemporary wind stress curl fields of the Arabian Sea, and (ii) using Canonical Correlation Analysis (CCA) to obtain the best relationship that relates the modes of wind stress curl to that of SST. Then we use these relationships along with the proxy data to reconstruct the modes of variability of wind stress curl and consequently its spatial field. The same approach is employed for reconstructing rainfall over the Indian subcontinent. *Von Storch and Zwiers* [2001] provide details of PCA and CCA techniques. A diagram of the main reconstruction steps is provided (Figure 6) and described in further detail in *Gill et al.* [2015, in review] where we used this to reconstruct SSTs and zonal winds over equatorial Pacific during the past 10,000 years. The approach is based on the methodologies and assumptions of [*Mann et al.*, 1998]. For the benefit of the readers we briefly describe the methodology below. Bold-faced uppercase variables denote matrices.

4.1. Reconstruction of Summer Monsoon Wind Stress Curl Fields

The contemporary de-trended full-field summer wind stress curl obtained as described above is organized into a matrix, $\boldsymbol{C}$ of dimension N x G, where N (= 65, 1949-2013) is the number of years, and G (=262) is the number of grid points.

Step (i). A Principal Component Analysis (PCA) is performed on the wind stress curl field over Arabian Sea, which decomposes the curl data into Principal Components (PCs), $\boldsymbol{Y}$, and eigenvectors, $\boldsymbol{U}$. The first four PCs of the wind stress curl field account for 22.1%, 10.6%, 9.7%, and 8.9%, respectively, of the total variance of the field (Figure 7a). The spatial patterns of these modes - empirical orthogonal functions (EOFs) - and PCs - are shown in Figure 8. The first EOF of the wind stress curl shows large values in the monsoonal jet region over the Arabian Sea, extending from the Somali coast to the western coast of India

Step (ii). The contemporary limited-field SST data at the locations of paleo-proxy data, which extend across the Indo-Pacific region (Figures 2-4), is organized as a matrix, $\boldsymbol{T}^{\dagger}$, of dimension N x P, where N is the length of the contemporary time period as before (1949-2013 therefore $N = 65$), and P (= 40) is the number of paleo-proxy records. A PCA on this limited SST field decomposes the data into PCs, $\boldsymbol{Y}^{\dagger}$, and eigenvectors, $\boldsymbol{U}^{\dagger}$, and reveals that the first four modes of the limited Indo-Pacific SST field account for 74.3%, 15.2%, 2.8%, and 1.8% of the limited field variance (Figure 7c). As seen in Figure 9 the first EOF is heavily weighted by changes in the eastern Pacific.

Step (iii). We retain a small number of PCs (NPC) from the contemporary full field PCA (*Step i*) and the limited field PCA (*Step ii*). To determine the optimal number of

PCs to retain, we compared the calibration statistics across a number of scenarios that involved retaining PCs that explain no less than 5% of the variance. With this criterion, $N_{PC} = 8$ (75.5% of the full field variance) for summer wind stress curl. A Canonical Correlation Analysis (CCA) was performed on the first eight retained PCs of wind stress curl with the first eight PCs of the limited SST field, which decomposes the PCs of each field into a matrix of canonical components (CCs) and a transformation matrix ($\boldsymbol{A}$ for curl; $\boldsymbol{B}$ for limited SSTs). Each of the eight pairs of canonical components ($\boldsymbol{S}$ and $\boldsymbol{S}^{\dagger}$) explains more of the joint variance than the next and is highly correlated. For example, the correlation coefficient of first CC, CC_1, of wind stress curl with CC_1 of the limited SST field is 0.81. Each CC of the full wind stress curl field is then linearly regressed with the corresponding CC of the limited SST field. The solution to the least squares optimization, $\hat{\boldsymbol{\beta}}$, will be used in *Step v* to reconstruct wind stress curl PCs.

Step (iv). For a given paleo time-period (e.g. 10 ka), the smoothed proxy data, $\boldsymbol{R}$, are contained in a 1 x P matrix (where P is the number of proxy records that have values for the given reconstruction period). Using the transpose of the eigenvalue transformation matrix from the PCA in *Step (ii)*, $[\boldsymbol{U}^{\dagger}]^T$, these proxy data are transformed into PCs, $\boldsymbol{Y}^{\boldsymbol{R}}$.

Step (v). Recall from *Steps ii* and *iii*, N_{PC} CC of the wind stress curl were obtained and the regression relationships between the two fields were formed. Reconstructed PCs, $\hat{\boldsymbol{Y}}$, of the full 10 ka wind stress curl field are obtained through expansion by multiplication of the first N_{PC} proxy PCs, $\boldsymbol{Y}^{\boldsymbol{R}}$, (from *Step v*) with the canonical transformation matrix from the canonical correlation, $\boldsymbol{A}$, and the least squares optimization solution, $\hat{\boldsymbol{\beta}}$, (from *Step iii*). In order to reconstruct the full field of the wind stress curl we need the remaining

(G minus N_{PC}) PCs. Since these capture less than 5% of the variance their mean values from the PCs of the contemporary period in *Step i* are used. This results in a full vector of PCs of wind stress curl of length G (=262), corresponding to given paleo time-period (e.g. 10 ka).

Step (vi). Finally, we obtain the reconstructed wind stress curl anomalies, $\hat{\boldsymbol{C}}$, by back transforming the reconstructed PCs, $\hat{\boldsymbol{Y}}$, with the eigenvector matrix of the full curl field, $\boldsymbol{U}$. *Steps iii-vi* are repeated for 8, 6, 4 and 2 ka. To avoid introducing bias, we choose not to reconstruct 0 ka, since several of the proxy records do not extend to 0 ka. The summer wind stress curl climatology is also shown on Figure 10.

4.2. Reconstruction of Summer Monsoon Rainfall Fields

For rainfall, the reconstruction process follows that for wind stress curl. There is no trend in the rainfall data that requires removal prior to the CCA-reconstruction. The seasonal average daily rainfall data is scaled (using means and standard deviations of each grid cell) and a PCA is performed. The first four modes explain 18.3%, 7.8%, 5.9%, and 5.1% of the total-field variance (Figure 11). The only difference in this methodology from that of the wind stress curl reconstruction is that $N = 104$ (for 1901-2004 data), $G = 357$ (grid cells over India), and we choose to retain the first four PCs ($N_{PC} = 4$) for the CCA, which jointly explain 37% of the variance. It should be underscored that this reconstruction focuses on capturing the variance present in the leading retained modes (i.e. the dominant 'signal'). For rainfall, only 37% of the total variance is captured, which is understandable given the highly variable nature of rainfall.

4.3. Model Calibration and Verification

As mentioned above, the reconstructions recover the dominant signal in the wind stress curl and rainfall fields, which account for a relatively small, but significant, percentage of the total variance. Thus, comparing the reconstructions to the full original data field will result in modest to poor skills. To be consistent, we compute the calibration and validation measures on the signal component of the original field. The signal components are obtained by projecting the PCs on to the retained eigenvectors. For example, let $\boldsymbol{X}$ be the original data matrix of size N x G, $\boldsymbol{Y}$ be the matrix of all the principal components also of size N x G and, $\boldsymbol{U_R}$ be the reduced eigenvector matrix of size G x G with the first N_{PC} columns containing the eigenvectors of the first N_{PC} modes and zero for the rest. The signal component of the original data $\boldsymbol{X_R}$ is obtained as: $\boldsymbol{X_R} = [\boldsymbol{Y}][\boldsymbol{U_R}]$.

Model calibration is performed on the signal components at each grid point using the 'resolved variance' statistic, β, given by:

$$\beta = 1 - \frac{\sum (y - \hat{y})^2}{\sum y^2} \tag{1}$$

where y is the contemporary signal data obtained in $\boldsymbol{X_R}$ above, and $\hat{y}$ is the reconstructed signal data for the full period. We also compared the squared correlation, R^2, between y and $\hat{y}$ at each grid point. These two statistics assess the reliability of the procedure in reproducing the contemporary signal data (See *Gill et al.* [2015, in review] and *Mann et al.* [1998] for more details on these statistics). The β-statistic serves as a measure of the resolved variance: for a perfect fit y is equal to $\hat{y}$ resulting in β =1, for a bad fit y and $\hat{y}$ are not equal and uncorrelated, leading to β =-1.

For reconstructions (Figure 12, top left) of the wind stress curl signal (first eight PCs), $\beta \geq 0.25$ in most of the monsoon jet region and smaller values characterize scattered areas across the Arabian Sea. The quality of reconstructions is perhaps better observed in the R^2 plot in regions where R^2 >0.25 (Figure 12, top right). For rainfall (Figure 12, bottom left) reconstructions the variability of the rainfall signal (first four PCs) are better captured than those for wind stress curl, for β >0.75 and R^2 >0.8 (Figure 12, bottom right).

As additional calibration, we compare reconstructions for two example years, (1) 1988-1989 - a strong La Niña year, and (2) 1997-1998 - a strong El Niño year [*Sontakke et al.*, 1993], with observations for them. We remind that the comparisons are made on the signal the first eight PCs for wind stress curl and first four PCs for the rainfall. For both periods, the general patterns of winds are captured in the key regions, if the strengths are underestimated. For example, in the La Niña summer of 1988 (Figure 13, top left), positive anomalies in wind stress curl, indicative of ocean upwelling, extended from the Yemen and northern Somali coastlines across the Arabian Sea and along the western border of India. This zone of positive anomalies was neighbored to the north and south by negative anomalies, indicative of ocean downwelling zones. The reconstruction captures the correct signs and similar spatial extents of these anomalies, but with positive magnitudes underestimated in the upwelling zone. In terms of rainfall, the summer of 1988 was interesting: although AISMR, a country-wide average monsoon rainfall index, reports an above average monsoon season, there was deficit rainfall in the north central region (Figure 13, top right). Typically, during La Niña, one would expect excess rainfall across

the core monsoon region, which makes this particular year unusual. Despite this, the reconstructed rainfall anomaly field shows a similar pattern to that of observed anomalies, capturing the dry anomalies just west of Bangladesh, albeit with muted magnitudes.

For the El Niño summer of 1997, a band of strongly negative anomalies of wind stress curl (-4 x 10^{-8} kg m^{-2} s^{-2}) extends from the Yemen and northern Somali coastlines across the Arabian Sea to the southern half of the Indian border (Figure 13, bottom left). This zone of negative anomalies, and down welling, is neighbored to the north by positive (upwelling) anomalies that extend from Oman to the northern half of the Indian border and to the south by a second zone that encompasses the western half of the equatorial Arabian Sea. This pattern is mostly captured, with the exception of the northern positive anomalies (upwelling). Magnitudes of the negative wind stress curl zone are underestimated. The rainfall reconstruction captures the main signal of deficit rainfall, but with negative rainfall anomalies across India that are more homogeneous than observed anomalies (Figure 13, bottom right).

For independent verification we fitted the modes using 1980-2013 for wind stress curl and 1980-2004 for rainfall and then reconstructed the signal for the earlier periods (1949-1979 for wind stress curl and 1901-1979 for rainfall). The verification maps for the two fields resemble the calibration maps (Figure 14). For wind stress curl (Figure 14, top panels) the verification skills are poor (β <0) over the Arabian Sea, but for rainfall, values of β >0.75 and R^2 >0.75 show skill across the country (Figure 13, bottom panels).

5. Multi-Proxy Reconstruction of Holocene Summer Wind Stress Curl and Rainfall Fields

The summer climatology of wind stress curl over the Arabian Sea region (Figure 15, top) includes a zone of positive wind stress curl, indicative of ocean upwelling, that is strongest between Yemen and Somalia, and extends but weakens across the northern Arabian Sea to the northwest coast of India. South of this, the summer wind stress curl is negative, with strongest negative values along the eastern coast of Somalia. Reconstructions of wind stress curl at 10, 6, 8, 4, and 2 ka are presented as percentage change from the present day climatology (Figure 15, bottom). At 10 ka (Figure 15, bottom right), strongest positive wind stress curl anomalies (upwelling) of 30% greater than present day are shown off the coast of Oman and central Somalia, extending and increasing to more than 50% greater than present day in the northeast region of the Arabian Sea. A band of negative wind stress curl extends from the tip of the northern Somali coastline ($\sim$ 15% less than present day) to the southern half of the Indian coastline (at least 50% less than present day). This general pattern remains similar throughout the Holocene, but gradually decreases in magnitude from 8 to 6 ka. By 4 to 2 ka, both positive and negative anomalies are minimal, barely exceeding 1 x 10^{-8} kg m^{-2} s^{-2}.

We calculated the percentage change in rainfall from present for 10, 8, 6, 4, and 2 ka and shown in Figure 16. The 10 ka reconstruction suggests that compared to present day: (a) most of Rajasthan and northern India should have received 40% greater precipitation, with some areas parts up to 60% greater precipitation, (b) the regions of the Ganges and Godavari River Basins (Figure 1) received about 20% greater precipitation, and (c) the rain shadow region of the Western Ghats, along with North East India, received less

rainfall ($\sim$ 25%). Note that *Sukumar et al.* [1993] had inferred relative arid conditions in this region when Rajasthan was wet. Throughout 10 to 6 ka, this pattern changes little. By 4 ka, percentage differences in rainfall over Rajasthan and Northern India had decreased to 30% greater than present-day, but the central Ganges and Godavari regions remain at about 20% greater precipitation than present day. At 2 ka, precipitation across the core monsoon region does not exceed 10-20% greater than present day.

Although the strength of a CCA method derives from its ability in isolating dominant signals in a system, its biggest weakness is in dealing with uncertainties. Unfortunately, uncertainties in the reconstruction of PCs, eigenvalues, and eigenvectors cannot be robustly treated easily and are difficult to obtain without drowning out the dominant signal in noise. We quantify uncertainty on the PCs of the dominant signal by calculating the standard error between the signal for an observed period and the signal of the reconstruction (Figure 17). Standard errors in both wind stress curl and rainfall are small (within 2% of present day values), which implies that the reconstruction of the signal is robust. We emphasize, however, that this represents the uncertainty in only the dominant signal, not the total uncertainty in the entire field.

6. Comparisons of Reconstructions to Proxy Records

Recall from Figure 1 that a reconstruction of *G. bulloides* has been used to infer enhanced upwelling off the coast of Oman (site OPD-732A) during early Holocene, which has been used to suggest a weakening of the monsoon winds since 10 ka [*Gupta et al.*, 2003]. The interpretation follows the logic that when the monsoon jet is strong, positive wind stress curl across the western Arabian Sea coastlines induces upwelling and a flux of

cold nutrient-rich water to the surface. This nutrient-rich water allows surface dwelling organisms, such as *G. bulloides*, to bloom. Reconstructed summer wind stress curl anomalies at the ODP-732A site (Figure 18, blue) compare well to the *Gupta et al.* [2003] *G. bulloides* time series (Figure 18, black), in the timing and trends of suggested upwelling. The *G. bulloides* record peaks at 8 ka, but is high from 10 to 8 ka. The reconstructed wind stress curl is consistently high throughout 10 to 8 ka, and decreases only slightly throughout that period. Following 8 ka, the *G. bulloides* record monotonically decreases to 2 ka. Although the reconstructed wind stress curl does not decrease at a constant rate, anomalies lessen from 8 to 6 ka, and from 4 ka to present day, with a minimum at present day.

The proxy data that suggest enhanced early- to mid-Holocene rainfall over the Indian subcontinent tend to cluster in defined regions of India (Figure 1). For example, most of the evidence from lakes comes from the northwestern region of Rajasthan, which is also near the 63KA proxy record recording discharge from the Indus River Basin [*Staubwasser et al.*, 2003]. Another region is the Godavari River Basin, which extends across central India from the Western Ghats to its mouth at 16A (Figure 1). As shown in the spatial reconstructions, the Indo-Gangetic Plains located along the northeastern border of India saw approximately 20% more rainfall during the early Holocene. With this information in mind, we define six regions over India, for which we aim to reconstruct mean daily monsoon rainfall time series: Northern India, Rajasthan, Western Ghats, Indo-Gangetic Plains, NE India, and Godavari (Figure 19). For each region, mean 1901-2004 daily summer rainfall time series are averaged over the regions defined in Figure 18. We then

regressed these time series as functions of the first four limited-field PCs from *Step (ii)* (Figure 9). These functional relationships, along with the paleo PCs from *Step (iii)*, are used to predict rainfall for each 1000-year period from 10 to 1 ka (Figure 19). Standard errors from the regression model fit provide errors on the rainfall reconstructions.

Among interesting features, first, most of the records reveal greater precipitation than in the present day during the early- and mid-Holocene, as reflected in the spatial CCA reconstruction (Figure 19). The one record that shows the opposite trend is Northeast India, which is consistent with both the spatial reconstruction and also contemporary patterns. North East India is known [e.g. *Guhathakurta and Rajeevan*, 2008] to be out of phase with the rest of the core monsoon region in terms of interannual variability (see the first EOF of rainfall in Figure 11), in that its relationship with ENSO (higher rainfall during El Niño years) is opposite to that of the core monsoon region (lower rainfall during El Niño years). Additionally, during the late Holocene when most records in the core monsoon region suggest aridification, the estimated precipitation for North East India is near that of the present day, if not slightly above, which would be consistent with a return of ENSO variability. Second, the seemingly monotonic decrease in rainfall since 10 ka suggested by the spatial reconstruction (Figure 16) looks less monotonic in the time series reconstructions. For instance, the Indo-Gangetic Plains time series shows greater precipitation than present day only during 10 to 6 ka. This is consistent with proxy records representative of runoff from the Ganges River basin: (1) *Kudrass et al.* [2001] cite a minimum in salinity from the early- to mid-Holocene that gradually increases to present day, and (2) *Goodbred and Kuehl* [2000] cite greatest sediment discharge between

11 and 7 ka. For the Godavari River Basin, the period of wetness extends to 3 ka, which is consistent with *Ponton et al.* [2012] who cite increased salinity past 3 ka. The period of wetness for Rajasthan extended from 10 to 4 ka, but seems more prominent in the earlier half of that time period.

A hydrological lake model [*Gill et al.*, 2015b] revealed that average annual precipitation 40-65% greater than present day was necessary to sustain Lake Sambhar in Rajasthan India (Figure 1). Reconstructions for Rajasthan of both the spatial pattern (Figure 16) and the appropriate Holocene time series (Figure 19) suggest that, although uncertainty is large, it is possible that ENSO teleconnections during an early- to mid-Holocene La Niña-like state contributed enough summer rainfall to Rajasthan to explain the enhanced wetness recorded by lake proxy records.

The uncertainties on the each time series rainfall reconstruction is large, in part, because the PC models must predict rainfall outside that of the observed range. In most cases, the large uncertainties make these trends marginally significant. At the least, these reconstructions suggest that it is within the realm of possibility for equatorial Pacific SSTs to externally force increased wetness over India.

7. Discussion

A total of forty proxy SST records (Mg/Ca and $U_{37}^{k'}$) that span the west Pacific, east Pacific, Arabian Sea, and Bay of Bengal are used in a reduced dimension methodology to reconstruct the full field dominant signal of Indian summer monsoon wind stress curl and rainfall at 10, 8, 6, 4 and 2 ka. The reconstructions reveal greatest wind stress curl and

rainfall anomalies, as compared to present day, at 10 ka. These anomalies weaken and lessen throughout the mid- and late- Holocene.

These reconstructions are consistent with a marine proxy record off the coast of Oman [*Gupta et al.*, 2003] that suggests enhanced upwelling during the early Holocene as compared to late Holocene. Additionally, average rainfall time series for the past 10 ka for six regions throughout India (Northern India, Rajasthan, Western Ghats, Indo-Gangetic Plains, Northeast India, and the Godavari Basin) are reconstructed using the PCs from the multi-proxy limited field. The rainfall reconstructions are consistent with many marine and continental proxy records that suggest enhanced rainfall during the early- to mid-Holocene as compared to late Holocene. Although most rainfall time series reconstructions suggest greatest precipitation at 10 ka, they reveal slight differences in the timing of each region that can be applied to various proxy records for precipitation and monsoon strength that have been reconstructed across the Indian subcontinent Figure 1.

The significance of these findings lies in the fact that only the patterns of wind stress curl and rainfall tied to Indo-Pacific SSTs are reconstructed. Therefore, although these findings do not consider the role on greater insolation over India on winds and rainfall in the early Holocene, they imply that it is possible that teleconnections from the tropical Pacific wrote a dominant signal on early to mid-Holocene Indian monsoon wetness. Accordingly, the return of ENSO variability in the late Holocene might be responsible for the aridification over India at that time.

Acknowledgments. ...

References

Achyuthan, H., J. Quade, L. Roe, and C. Placzek (2007), Stable isotopic composition of pedogenic carbonates from the eastern margin of the thar desert, rajasthan, india, *Quaternary International*, *162*, 50–60.

Allan, R. J., J. A. Lindesay, and C. J. Reason (1995), Multidecadal variability in the climate system over the indian ocean region during the austral summer, *Journal of Climate*, *8*(7), 1853–1873.

Anand, P., H. Elderfield, and M. H. Conte (2003), Calibration of mg/ca thermometry in planktonic foraminifera from a sediment trap time series, *Paleoceanography*, *18*(2).

Bard, E., F. Rostek, and C. Sonzogni (1997), Interhemispheric synchrony of the last deglaciation inferred from alkenone palaeothermometry, *Nature*, *385*(6618), 707–710.

Beaufort, L., S. Kaars, F. Bassinot, and V. Moron (2010), Past dynamics of the australian monsoon: precession, phase and links to the global monsoon concept, *Climate of the Past*, *6*(5), 695–706.

Bemis, E., H. J. Spero, J. Bijma, and D. W. Lea (1998), Reevaluation of the oxygen isotopic composition of planktonic foraminifera: Experimental results and revised paleotemperature equations, *Paleoceanography*, *13*(2), 150–160.

Benway, H. M., A. C. Mix, B. A. Haley, and G. P. Klinkhammer (2006), Eastern pacific warm pool paleosalinity and climate variability: 0–30 kyr, *Paleoceanography*, *21*(3).

Bolliet, T., A. Holbourn, W. Kuhnt, C. Laj, C. Kissel, L. Beaufort, M. Kienast, N. Andersen, and D. Garbe-Schönberg (2011), Mindanao dome variability over the last 160 kyr: Episodic glacial cooling of the west pacific warm pool, *Paleoceanography*, *26*(1).

Brassell, S., G. Eglinton, I. Marlowe, U. Pflaumann, and M. Sarnthein (1986), Molecular stratigraphy: a new tool for climatic assessment, *Nature*, *320*, 129–133.

Bryson, R. A., and A. Swain (1981), Holocene variations of monsoon rainfall in rajasthan, *Quaternary Research*, *16*(2), 135–145.

Chazen, C. R., M. A. Altabet, and T. D. Herbert (2009), Abrupt mid-holocene onset of centennial-scale climate variability on the peru-chile margin, *Geophysical Research Letters*, *36*(18).

Clement, A., R. Seager, and M. Cane (1999), Orbital controls on the el niño/southern oscillation and the tropical climate, *Paleoceanography*, *14*(4), 441–456.

Clement, A. C., R. Seager, and M. A. Cane (2000), Suppression of el niño during the mid-holocene by changes in the earth's orbit, *Paleoceanography*, *15*(6), 731–737.

Conroy, J. L., J. T. Overpeck, J. E. Cole, T. M. Shanahan, and M. Steinitz-Kannan (2008), Holocene changes in eastern tropical pacific climate inferred from a galápagos lake sediment record, *Quaternary Science Reviews*, *27*(11), 1166–1180.

Conte, M. H., M.-A. Sicre, C. Rühlemann, J. C. Weber, S. Schulte, D. Schulz-Bull, and T. Blanz (2006), Global temperature calibration of the alkenone unsaturation index (uk 37) in surface waters and comparison with surface sediments, *Geochemistry, Geophysics, Geosystems*, *7*(2).

Curry, W., D. Ostermann, M. Guptha, and V. Ittekkot (1992), Foraminiferal production and monsoonal upwelling in the arabian sea: evidence from sediment traps, *Geological Society, London, Special Publications*, *64*(1), 93–106.

de Garidel-Thoron, T., Y. Rosenthal, F. Bassinot, and L. Beaufort (2005), Stable sea surface temperatures in the western pacific warm pool over the past 1.75 million years, *Nature*, *433*(7023), 294–298.

de Garidel-Thoron, T., Y. Rosenthal, L. Beaufort, E. Bard, C. Sonzogni, and A. C. Mix (2007), A multiproxy assessment of the western equatorial pacific hydrography during the last 30 kyr, *Paleoceanography*, *22*(3).

Dekens, P. S., D. W. Lea, D. K. Pak, and H. J. Spero (2002), Core top calibration of mg/ca in tropical foraminifera: Refining paleotemperature estimation, *Geochemistry, Geophysics, Geosystems*, *3*(4), 1–29.

Deotare, B., M. Kajale, S. Rajaguru, S. Kusumgar, A. Jull, and J. Donahue (2004), Palaeoenvironmental history of bap-malar and kanod playas of western rajasthan, thar desert, *Journal of Earth System Science*, *113*(3), 403–425.

Doose-Rolinski, H., U. Rogalla, G. Scheeder, A. Lückge, and U. Rad (2001), High-resolution temperature and evaporation changes during the late holocene in the north-eastern arabian sea, *Paleoceanography*, *16*(4), 358–367.

Emile-Geay, J., M. Cane, R. Seager, A. Kaplan, and P. Almasi (2007), El niño as a mediator of the solar influence on climate, *Paleoceanography*, *22*(3).

Enzel, Y., L. Ely, S. Mishra, R. Ramesh, R. Amit, B. Lazar, S. Rajaguru, V. Baker, and A. Sandler (1999), High-resolution holocene environmental changes in the thar desert, northwestern india, *Science*, *284*(5411), 125–128.

Fleitmann, D., S. J. Burns, M. Mudelsee, U. Neff, J. Kramers, A. Mangini, and A. Matter (2003), Holocene forcing of the indian monsoon recorded in a stalagmite from

532 southern oman, *Science*, *300*(5626), 1737–1739.

533 Fleitmann, D., S. J. Burns, A. Mangini, M. Mudelsee, J. Kramers, I. Villa, U. Neff, A. A.
534 Al-Subbary, A. Buettner, D. Hippler, et al. (2007), Holocene itcz and indian monsoon
535 dynamics recorded in stalagmites from oman and yemen (socotra), *Quaternary Science*
536 *Reviews*, *26*(1), 170–188.

537 Gill, E., B. Rajagopalan, and P. Molnar (2015a), Subseasonal variations in spatial signa-
538 tures of enso on the indian summer monsoon from 1901 to 2009, *Journal of Geophysical*
539 *Research, Atmospheres*.

540 Gill, E., B. Rajagopalan, and P. Molnar (2015b), An assessment of the mean annual
541 precipitation neede to sustain mid-holocene lakes in rajasthan, india, *The Holocene*.

542 Gill, E., B. Rajagopalan, P. Molnar, Y. Kushnir, and T. Marchitto (2015, in review),
543 Subseasonal variations in spatial signatures of enso on the indian summer monsoon
544 from 1901 to 2009, *Paleoceanography*.

545 Goodbred, S. L., and S. A. Kuehl (2000), Enormous ganges-brahmaputra sediment
546 discharge during strengthened early holocene monsoon, *Geology*, *28*(12), 1083–1086.

547 Govil, P., and P. D. Naidu (2010), Evaporation-precipitation changes in the eastern
548 arabian sea for the last 68 ka: Implications on monsoon variability, *Paleoceanography*,
549 *25*(1).

550 Guhathakurta, P., and M. Rajeevan (2008), Trends in the rainfall pattern over india,
551 *International Journal of Climatology*, *28*(11), 1453–1469.

552 Gupta, A. K., D. M. Anderson, and J. T. Overpeck (2003), Abrupt changes in the asian
553 southwest monsoon during the holocene and their links to the north atlantic ocean,

Nature, *421*(6921), 354–357.

Hastings, D., M. Kienast, S. Steinke, and A. Whitko (2001), A comparison of three independent paleotemperature estimates from a high resolution record of deglacial sst records in the tropical south china sea, in *AGU Fall Meeting Abstracts*, vol. 1, p. 10.

Herbert, T. (2003), Alkenone paleotemperature determinations, Elsevier.

Ihara, C., Y. Kushnir, and M. A. Cane (2008), Warming trend of the indian ocean sst and indian ocean dipole from 1880 to 2004*, *Journal of Climate*, *21*(10), 2035–2046.

Ivanochko, T. S., R. S. Ganeshram, G.-J. A. Brummer, G. Ganssen, S. J. Jung, S. G. Moreton, and D. Kroon (2005), Variations in tropical convection as an amplifier of global climate change at the millennial scale, *Earth and Planetary Science Letters*, *235*(1), 302–314.

Kajale, M., and B. Deotare (1997), Late quaternary environmental studies on salt lakes in western rajasthan, india: a summarised view, *Journal of Quaternary Science*, *12*(5), 405–412.

Kalnay, E., M. Kanamitsu, R. Kistler, W. Collins, D. Deaven, L. Gandin, M. Iredell, S. Saha, G. White, J. Woollen, et al. (1996), The ncep/ncar 40-year reanalysis project, *Bulletin of the American meteorological Society*, *77*(3), 437–471.

Kienast, M., S. Steinke, K. Stattegger, and S. Calvert (2001), Synchronous tropical south china sea sst change and greenland warming during deglaciation, *Science*, *291*(5511), 2132–2134.

Kienast, M., S. S. Kienast, S. E. Calvert, T. I. Eglinton, G. Mollenhauer, R. François, and A. C. Mix (2006), Eastern pacific cooling and atlantic overturning circulation

during the last deglaciation, *Nature*, *443*(7113), 846–849.

Kim, J.-H., N. Rimbu, S. J. Lorenz, G. Lohmann, S.-I. Nam, S. Schouten, C. Rühlemann, and R. R. Schneider (2004), North pacific and north atlantic sea-surface temperature variability during the holocene, *Quaternary Science Reviews*, *23*(20), 2141–2154.

Koutavas, A., and J. P. Sachs (2008), Northern timing of deglaciation in the eastern equatorial pacific from alkenone paleothermometry, *Paleoceanography*, *23*(4).

Koutavas, A., J. Lynch-Stieglitz, T. M. Marchitto, and J. P. Sachs (2002), El nino-like pattern in ice age tropical pacific sea surface temperature, *Science*, *297*(5579), 226–230.

Koutavas, A., G. C. Olive, J. Lynch-Stieglitz, et al. (2006), Mid-holocene el niño–southern oscillation (enso) attenuation revealed by individual foraminifera in eastern tropical pacific sediments, *Geology*, *34*(12), 993–996.

Krishna Kumar, K., M. Soman, and K. R. Kumar (1995), Seasonal forecasting of indian summer monsoon rainfall: a review, *Weather*, *50*(12), 449–467.

Krishna Kumar, K., B. Rajagopalan, M. Hoerling, G. Bates, and M. Cane (2006), Unraveling the mystery of indian monsoon failure during el nino, *Science*, *314*(5796), 115–119.

Krishna Kumar, K., K. Kamala, B. Rajagopalan, M. P. Hoerling, J. K. Eischeid, S. Patwardhan, G. Srinivasan, B. Goswami, and R. Nemani (2011), The once and future pulse of indian monsoonal climate, *Climate dynamics*, *36*(11-12), 2159–2170.

Krishnamurthy, V., and B. P. Kirtman (2003), Variability of the indian ocean: Relation to monsoon and enso, *Quarterly Journal of the Royal Meteorological Society*, *129*(590),

598 1623–1646.

599 Kudrass, H., A. Hofmann, H. Doose, K. Emeis, and H. Erlenkeuser (2001), Modulation
600 and amplification of climatic changes in the northern hemisphere by the indian summer
601 monsoon during the past 80 ky, *Geology*, *29*(1), 63–66.

602 Kutzbach, J., and B. Otto-Bliesner (1982), The sensitivity of the african-asian mon-
603 soonal climate to orbital parameter changes for 9000 years bp in a low-resolution
604 general circulation model, *Journal of the Atmospheric Sciences*, *39*(6), 1177–1188.

605 Kutzbach, J. E. (1981), Monsoon climate of the early holocene: climate experiment
606 with the earths orbital parameters for 9000 years ago, *Science*, *214*(4516), 59–61.

607 Lea, D. W., and P. A. Martin (1996), A rapid mass spectrometric method for the simul-
608 taneous analysis of barium, cadmium, and strontium in foraminifera shells, *Geochimica*
609 *et Cosmochimica Acta*, *60*(16), 3143–3149.

610 Lea, D. W., T. A. Mashiotta, and H. J. Spero (1999), Controls on magnesium and
611 strontium uptake in planktonic foraminifera determined by live culturing, *Geochimica*
612 *et Cosmochimica Acta*, *63*(16), 2369–2379.

613 Lea, D. W., D. K. Pak, and H. J. Spero (2000), Climate impact of late quaternary
614 equatorial pacific sea surface temperature variations, *Science*, *289*(5485), 1719–1724.

615 Lea, D. W., D. K. Pak, C. L. Belanger, H. J. Spero, M. A. Hall, and N. J. Shackleton
616 (2006), Paleoclimate history of galapagos surface waters over the last 135,000 yr,
617 *Quaternary Science Reviews*, *25*(11), 1152–1167.

618 Leduc, G., L. Vidal, K. Tachikawa, F. Rostek, C. Sonzogni, L. Beaufort, and E. Bard
619 (2007), Moisture transport across central america as a positive feedback on abrupt

620 climatic changes, *Nature*, *445*(7130), 908–911.

621 Leduc, G., R. Schneider, J.-H. Kim, and G. Lohmann (2010), Holocene and eemian sea
622 surface temperature trends as revealed by alkenone and mg/ca paleothermometry,
623 *Quaternary Science Reviews*, *29*(7), 989–1004.

624 Levi, C., L. Labeyrie, F. Bassinot, F. Guichard, E. Cortijo, C. Waelbroeck, N. Cail-
625 lon, J. Duprat, T. de Garidel-Thoron, and H. Elderfield (2007), Low-latitude hydro-
626 logical cycle and rapid climate changes during the last deglaciation, *Geochemistry,*
627 *Geophysics, Geosystems*, *8*(5).

628 Li, C., and M. Yanai (1996), The onset and interannual variability of the asian summer
629 monsoon in relation to land-sea thermal contrast, *Journal of Climate*, *9*(2), 358–375.

630 Liu, Z., J. Kutzbach, and L. Wu (2000), Modeling climate shift of el nino variability in
631 the holocene, *Geophysical Research Letters*, *27*(15), 2265–2268.

632 Loader, C. R., et al. (1996), Local likelihood density estimation, *The Annals of Statistics*,
633 *24*(4), 1602–1618.

634 Lückge, A., M. Mohtadi, C. Rühlemann, G. Scheeder, A. Vink, L. Reinhardt, and
635 M. Wiedicke (2009), Monsoon versus ocean circulation controls on paleoenvironmen-
636 tal conditions off southern sumatra during the past 300,000 years, *Paleoceanography*,
637 *24*(1).

638 Mann, M. E., R. S. Bradley, and M. K. Hughes (1998), Global-scale temperature pat-
639 terns and climate forcing over the past six centuries, *Nature*, *392*(6678), 779–787.

640 Mohtadi, M., S. Steinke, A. Lückge, J. Groeneveld, and E. C. Hathorne (2010), Glacial to
641 holocene surface hydrography of the tropical eastern indian ocean, *Earth and Planetary*

642 *Science Letters*, *292*(1), 89–97.

643 Moy, C. M., G. O. Seltzer, D. T. Rodbell, and D. M. Anderson (2002), Variability of el
644 niño/southern oscillation activity at millennial timescales during the holocene epoch,
645 *Nature*, *420*(6912), 162–165.

646 Müller, P. J., G. Kirst, G. Ruhland, I. von Storch, and A. Rosell-Melé (1998), Calibration
647 of the alkenone paleotemperature index u 37 k based on core-tops from the eastern
648 south atlantic and the global ocean (60 n-60 s), *Geochimica et Cosmochimica Acta*,
649 *62*(10), 1757–1772.

650 Neff, U., S. Burns, A. Mangini, M. Mudelsee, D. Fleitmann, and A. Matter (2001),
651 Strong coherence between solar variability and the monsoon in oman between 9 and
652 6 kyr ago, *Nature*, *411*(6835), 290–293.

653 Nürnberg, D., J. Bijma, and C. Hemleben (1996), Assessing the reliability of magne-
654 sium in foraminiferal calcite as a proxy for water mass temperatures, *Geochimica et*
655 *Cosmochimica Acta*, *60*(5), 803–814.

656 Pahnke, K., J. P. Sachs, L. Keigwin, A. Timmermann, and S.-P. Xie (2007), Eastern
657 tropical pacific hydrologic changes during the past 27,000 years from d/h ratios in
658 alkenones, *Paleoceanography*, *22*(4).

659 Parthasarathy, B., and G. Pant (1985), Seasonal relationships between indian summer
660 monsoon rainfall and the southern oscillation, *Journal of climatology*, *5*(4), 369–378.

661 Pelejero, C., and J. O. Grimalt (1997), The correlation between the uk'37 index and
662 sea surface temperatures in the warm boundary: The south china sea, *Geochimica et*
663 *Cosmochimica Acta*, *61*(22), 4789–4797.

664 Pelejero, C., J. O. Grimalt, S. Heilig, M. Kienast, L. Wang, et al. (1999), High-resolution
665 uk37 temperature reconstructions in the south china sea over the past 220 kyr, *Pale-*
666 *oceanography*, *14*(2), 224–231.

667 Pena, L., I. Cacho, P. Ferretti, and M. Hall (2008), El niño–southern oscillation–like vari-
668 ability during glacial terminations and interlatitudinal teleconnections, *Paleoceanog-*
669 *raphy*, *23*(3).

670 Ponton, C., L. Giosan, T. I. Eglinton, D. Q. Fuller, J. E. Johnson, P. Kumar, and T. S.
671 Collett (2012), Holocene aridification of india, *Geophysical Research Letters*, *39*(3).

672 Prahl, F. G., L. A. Muehlhausen, and D. L. Zahnle (1988), Further evaluation of long-
673 chain alkenones as indicators of paleoceanographic conditions, *Geochimica et Cos-*
674 *mochimica Acta*, *52*(9), 2303–2310.

675 Prasad, S., S. Kusumgar, and S. Gupta (1997), A midlate holocene record of palaeocli-
676 matic changes from nal sarovara palaeodesert margin lake in western india, *Journal*
677 *of Quaternary Science*, *12*, 153–159.

678 Prell, W., and W. Curry (1981), Faunal and isotopic indices of monsoonal upwelling-
679 western arabian sea, *Oceanologica Acta*, *4*(1), 91–98.

680 Rajagopalan, B., and P. Molnar (2013), Signatures of tibetan plateau heating on indian
681 summer monsoon rainfall variability, *Journal of Geophysical Research: Atmospheres*,
682 *118*(3), 1170–1178.

683 Rajeevan, M., J. Bhate, J. Kale, and B. Lal (2006), High resolution daily gridded
684 rainfall data for the indian region: Analysis of break and active monsoon spells.,
685 *Current Science (00113891)*, *91*(3).

686 Rein, B., A. Lückge, L. Reinhardt, F. Sirocko, A. Wolf, and W.-C. Dullo (2005), El niño
687 variability off peru during the last 20,000 years, *Paleoceanography*, *20*(4).
688 Riedinger, M. A., M. Steinitz-Kannan, W. M. Last, and M. Brenner (2002), A 6100 14
689 c yr record of el niño activity from the galápagos islands, *Journal of Paleolimnology*,
690 *27*(1), 1–7.
691 Rodbell, D. T., G. O. Seltzer, D. M. Anderson, M. B. Abbott, D. B. Enfield, and J. H.
692 Newman (1999), An˜ 15,000-year record of el niño-driven alluviation in southwestern
693 ecuador, *Science*, *283*(5401), 516–520.
694 Rosenthal, Y., and G. P. Lohmann (2002), Accurate estimation of sea surface temper-
695 atures using dissolution-corrected calibrations for mg/ca paleothermometry, *Paleo-*
696 *ceanography*, *17*(3), 16–1.
697 Rosenthal, Y., D. W. Oppo, and B. K. Linsley (2003), The amplitude and phasing of
698 climate change during the last deglaciation in the sulu sea, western equatorial pacific,
699 *Geophysical Research Letters*, *30*(8).
700 Rostek, F., G. Ruhland, F. Bassinot, P. Müller, L. Labeyrie, Y. Lancelot, and E. Bard
701 (1993), Reconstructing sea surface temperature and salinity using¿ lso and alkenone
702 records, *Nature*, *364*, 319–321.
703 Rostek, F., E. Bard, L. Beaufort, C. Sonzogni, and G. Ganssen (1997), Sea surface
704 temperature and productivity records for the past 240 kyr in the arabian sea, *Deep*
705 *Sea Research Part II: Topical Studies in Oceanography*, *44*(6), 1461–1480.
706 Roxy, M. K., K. Ritika, P. Terray, and S. Masson (2014), The curious case of indian
707 ocean warming, *Journal of Climate*, (2014).

Sandweiss, D. H., J. B. Richardson, E. J. Reitz, H. B. Rollins, and K. A. Maasch (1996), Geoarchaeological evidence from peru for a 5000 years b.p. onset of el nio, *Science*, *273*(5281), 1531–1533.

Sandweiss, D. H., K. A. Maasch, R. L. Burger, J. B. Richardson, H. B. Rollins, and A. Clement (2001), Variation in holocene el niño frequencies: Climate records and cultural consequences in ancient peru, *Geology*, *29*(7), 603–606.

Saraswat, R., R. Nigam, S. Weldeab, A. Mackensen, and P. Naidu (2005), A first look at past sea surface temperatures in the equatorial indian ocean from mg/ca in foraminifera, *Geophysical research letters*, *32*(24).

Saraswat, R., D. W. Lea, R. Nigam, A. Mackensen, and D. K. Naik (2013), Deglaciation in the tropical indian ocean driven by interplay between the regional monsoon and global teleconnections, *Earth and Planetary Science Letters*, *375*, 166–175.

Sarkar, A., R. Ramesh, B. Somayajulu, R. Agnihotri, A. Jull, and G. Burr (2000), High resolution holocene monsoon record from the eastern arabian sea, *Earth and Planetary Science Letters*, *177*(3), 209–218.

Schulte, S., and P. J. Müller (2001), Variations of sea surface temperature and primary productivity during heinrich and dansgaard-oeschger events in the northeastern arabian sea, *Geo-Marine Letters*, *21*(3), 168–175.

Schulz, H., K.-C. Emeis, H. Erlenkeuser, U. von Rad, and C. Rolf (2002), The toba volcanic event and interstadial/stadial climates at the marine isotopic stage 5 to 4 transition in the northern indian ocean, *Quaternary Research*, *57*(1), 22–31.

729 Shukla, J., and D. Mooley (1987), Empirical prediction of the summer monsoon rainfall
730 over india, *Monthly Weather Review*, *115*(3), 695–704.

731 Shukla, J., and D. A. Paolino (1983), The southern oscillation and long-range forecasting
732 of the summer monsoon rainfall over india, *Monthly Weather Review*, *111*(9), 1830–
733 1837.

734 Singh, G., R. D. Joshi, and A. Singh (1972), Stratigraphic and radiocarbon evidence for
735 the age and development of three salt lake deposits in rajasthan, india, *Quaternary*
736 *Research*, *2*(4), 496–505.

737 Singh, G., S. Chopra, and A. Singh (1973), Pollen-rain from the vegetation of north-west
738 india, *New Phytologist*, *72*(1), 191–206.

739 Singh, G., R. Joshi, S. Chopra, and A. Singh (1974), Late quaternary history of veg-
740 etation and climate of the rajasthan desert, india, *Philosophical Transactions of the*
741 *Royal Society of London. B, Biological Sciences*, *267*(889), 467–501.

742 Singh, G., R. Wasson, and D. Agrawal (1990), Vegetational and seasonal climatic
743 changes since the last full glacial in the thar desert, northwestern india, *Review of*
744 *Palaeobotany and Palynology*, *64*(1), 351–358.

745 Smith, T. M., R. W. Reynolds, T. C. Peterson, and J. Lawrimore (2008), Improvements
746 to noaa's historical merged land-ocean surface temperature analysis (1880-2006), *Jour-*
747 *nal of Climate*, *21*(10), 2283–2296.

748 Sontakke, N., G. Pant, and N. Singh (1993), Construction of all-india summer monsoon
749 rainfall series for the period 1844-1991, *Journal of Climate*, *6*(9), 1807–1811.

Sonzogni, C., E. Bard, F. Rostek, R. Lafont, A. Rosell-Mele, and G. Eglinton (1997), Core-top calibration of the alkenone index vs sea surface temperature in the indian ocean, *Deep Sea Research Part II: Topical Studies in Oceanography*, *44*(6), 1445–1460.

Sonzogni, C., E. Bard, and F. Rostek (1998), Tropical sea-surface temperatures during the last glacial period: a view based on alkenones in indian ocean sediments, *Quaternary Science Reviews*, *17*(12), 1185–1201.

Staubwasser, M., F. Sirocko, P. Grootes, and M. Segl (2003), Climate change at the 4.2 ka bp termination of the indus valley civilization and holocene south asian monsoon variability, *Geophysical Research Letters*, *30*(8).

Steinke, S., M. Kienast, J. Groeneveld, L.-C. Lin, M.-T. Chen, and R. Rendle-Bühring (2008), Proxy dependence of the temporal pattern of deglacial warming in the tropical south china sea: toward resolving seasonality, *Quaternary Science Reviews*, *27*(7), 688–700.

Stott, L., C. Poulsen, S. Lund, and R. Thunell (2002), Super enso and global climate oscillations at millennial time scales, *Science*, *297*(5579), 222–226.

Stott, L., K. Cannariato, R. Thunell, G. H. Haug, A. Koutavas, and S. Lund (2004), Decline of surface temperature and salinity in the western tropical pacific ocean in the holocene epoch, *Nature*, *431*(7004), 56–59.

Sukumar, R., R. Ramoshr, R. Panti, and G. Rajagopalani (1993), A 5130 record of late, *Nature*, *364*, 19.

Swain, A., J. Kutzbach, and S. Hastenrath (1983), Estimates of holocene precipitation for rajasthan, india, based on pollen and lake-level data, *Quaternary Research*, *19*(1),

772 1–17.

773 Terray, P., and S. Dominiak (2005), Indian ocean sea surface temperature and el nino-
774 southern oscillation: A new perspective, *Journal of Climate*, *18*(9), 1351–1368.

775 Visser, K., R. Thunell, and L. Stott (2003), Magnitude and timing of temperature change
776 in the indo-pacific warm pool during deglaciation, *Nature*, *421*(6919), 152–155.

777 von Rad, U., M. Schaaf, K. H. Michels, H. Schulz, W. H. Berger, and F. Sirocko (1999),
778 A 5000-yr record of climate change in varved sediments from the oxygen minimum
779 zone off pakistan, northeastern arabian sea, *Quaternary Research*, *51*(1), 39–53.

780 Von Storch, H., and F. W. Zwiers (2001), *Statistical analysis in climate research*, Cam-
781 bridge university press.

782 Wasson, R., G. Smith, and D. Agrawal (1984), Late quaternary sediments, minerals,
783 and inferred geochemical history of didwana lake, thar desert, india, *Palaeogeography,*
784 *Palaeoclimatology, Palaeoecology*, *46*(4), 345–372.

785 Webster, P. (1987), The elementary monsoon, in *Monsoons*, edited by J. S. Fein and
786 P. L. Stephens, John Wiley and Sons.

787 Webster, P. J., V. O. Magana, T. Palmer, J. Shukla, R. Tomas, M. u. Yanai, and T. Ya-
788 sunari (1998), Monsoons: Processes, predictability, and the prospects for prediction,
789 *Journal of Geophysical Research: Oceans (1978–2012)*, *103*(C7), 14,451–14,510.

790 Wu, G., Y. Liu, Q. Zhang, A. Duan, T. Wang, R. Wan, X. Liu, W. Li, Z. Wang,
791 and X. Liang (2007), The influence of mechanical and thermal forcing by the tibetan
792 plateau on asian climate, *Journal of Hydrometeorology*, *8*(4), 770–789.

Zhao, M., C.-Y. Huang, C.-C. Wang, and G. Wei (2006), A millennial-scale u 37 k sea-surface temperature record from the south china sea (8 n) over the last 150 kyr: Monsoon and sea-level influence, *Palaeogeography, Palaeoclimatology, Palaeoecology*, *236*(1), 39–55.

Table 1. A list of the Mg/Ca-based proxy records from the western and eastern equatorial Pacific used in the SST and zonal wind reconstruction.

Record #	Core	Lat	Lon	Calibration	Reference
Western Equatorial Pacific (Figure 2, left)					
1	MD98 - 2176	-5.00	133.45	*Nürnberg et al.* [1996]	*Stott et al.* [2004]
2	MD98 - 2181	6.30	125.83	*Nürnberg et al.* [1996]	*Stott et al.* [2004]
3	MD98 - 2162	-4.69	117.90	*Hastings et al.* [2001]	*Visser et al.* [2003]
4	MD01 - 2390	6.64	113.41	*Dekens et al.* [2002]	*Steinke et al.* [2008]
5	MD97 - 2141	8.80	121.30	*Rosenthal and Lohmann* [2002]	*Rosenthal et al.* [2003]
6	MD97 - 2138 *	1.25	146.14	*de Garidel-Thoron et al.* [2005]	*de Garidel-Thoron et al.* [2007]
7	ODP - 806b	0.32	159.35	*Lea and Martin* [1996]	*Lea et al.* [2000]
8	MD98 - 2165	-9.65	118.34	*Dekens et al.* [2002]	*Levi et al.* [2007]
9	MD98 - 2170	-10.59	125.39	*Nürnberg et al.* [1996]	*Stott et al.* [2004]
10	MD06 - 3067	6.51	126.50	*Anand et al.* [2003]	*Bolliet et al.* [2011]
Eastern Equatorial Pacific (Figure 2, right)					
11	ODP - 1242	7.86	-83.61	*Anand et al.* [2003]	*Benway et al.* [2006]
12	TR163 - 22	0.52	-92.40	*Dekens et al.* [2002]	*Lea et al.* [2006]
13	ODP - 1240	0.02	-86.45	*Dekens et al.* [2002]	*Pena et al.* [2008]
14	V21 - 30 *	-1.22	-89.68	*Dekens et al.* [2002]	*Koutavas et al.* [2006]
15	V19 - 28 *	-2.51	-84.65	*Dekens et al.* [2002]	*Koutavas et al.* [2006]

Table 2. A list of the U^k_{37}-based proxy records from the western and eastern equatorial Pacific used in the SST and zonal wind reconstruction.

Record #	**Core**	**Lat**	**Lon**	**Calibration**	**Reference**
Western Equatorial Pacific (Figure 3, left)					
16	SO139 - 74KL	-6.54	103.83	*Conte et al.* [2006]	*Lückge et al.* [2009]
17	GIK 17964	6.16	112.21	*Müller et al.* [1998]	*Pelejero et al.* [1999]
18	GIK 18252-3	9.23	109.38	*Pelejero and Grimalt* [1997]	*Kienast et al.* [2001]
19	GIK 18287-3	5.65	110.65	*Pelejero and Grimalt* [1997]	*Kienast et al.* [2001]
20	MD97 - 2151	8.72	109.87	*Pelejero and Grimalt* [1997]	*Zhao et al.* [2006]
21	MD97 - 2138 *	1.25	146.14	*Prahl et al.* [1988]	*de Garidel-Thoron et al.* [2007]
Eastern Equatorial Pacific (Figure 3, right)					
22	MD02 - 2529	8.21	-84.12	*Sonzogni et al.* [1997]	*Leduc et al.* [2007]
23	KNR176 - JPC32	4.85	-77.96	*Prahl et al.* [1988]	*Pahnke et al.* [2007]
24	V19 - 27	-0.47	-82.67	*Prahl et al.* [1988]	*Koutavas and Sachs* [2008]
25	ME0005A - 24JC	1.50	-89.68	*Prahl et al.* [1988]	*Kienast et al.* [2006]
26	V21 - 30 *	-1.22	-89.68	*Prahl et al.* [1988]	*Koutavas and Sachs* [2008]
27	V19 - 30	-3.38	-83.52	*Prahl et al.* [1988]	*Koutavas and Sachs* [2008]
28	RC11 - 238	-1.52	-85.82	*Prahl et al.* [1988]	*Koutavas and Sachs* [2008]
29	V19 - 28 *	-2.51	-84.65	*Prahl et al.* [1988]	*Koutavas and Sachs* [2008]

Table 3. A list of the Mg/Ca- and $U_{37}^{k'}$-based proxy records from the Indian Ocean used in the summer monsoon wind and rainfall reconstructions.

Record #	**Core**	**Lat**	**Lon**	**Calibration**	**Reference**
Mg/Ca-based SST records (Figure 4, left)					
30	SK 237 - GC04	11.0	75.0	*Dekens et al.* [2002]	*Saraswat et al.* [2013]
31	GeoB 10029 - 4	-1.5	100.1	*Anand et al.* [2003]	*Mohtadi et al.* [2010]
32	GeoB 10038 - 4	-5.9	103.3	*Anand et al.* [2003]	*Mohtadi et al.* [2010]
33	SK 157 - GC04	2.4	78.0	*Dekens et al.* [2002]	*Saraswat et al.* [2005]
34	AA S9/21	14.5	72.7	*Bemis et al.* [1998]	*Govil and Naidu* [2010]
$U_{37}^{k'}$-based SST records (Figure 4, right)					
35	MD77 - 194	10.3	75.1	*Prahl et al.* [1988]	*Sonzogni et al.* [1998]
36	SO90 - 39KG	24.8	65.9	*Sonzogni et al.* [1997]	*von Rad et al.* [1999]; *Doose-Rolinski et al.* [2001]
37	MD85 - 668	0.02	46.0	*Prahl et al.* [1988]	*Bard et al.* [1997]
38	SO90 - 93KL	23.6	64.2	*Müller et al.* [1998]	*Schulz et al.* [2002]
39	SO90 - 136KL	23.1	66.5	*Müller et al.* [1998]	*Schulte and Müller* [2001]
40	SO93 - 126KL	20.0	90.0	*Sonzogni et al.* [1997]	*Kudrass et al.* [2001]
41	TY93 - 905	11.1	52.0	*Prahl et al.* [1988]	*Kim et al.* [2004]
42	TY93 - 929/P	13.7	53.3	*Prahl et al.* [1988]	*Rostek et al.* [1997]
43	SO139 - 74KL	-6.5	103.8	*Conte et al.* [2006]	*Lückge et al.* [2009]

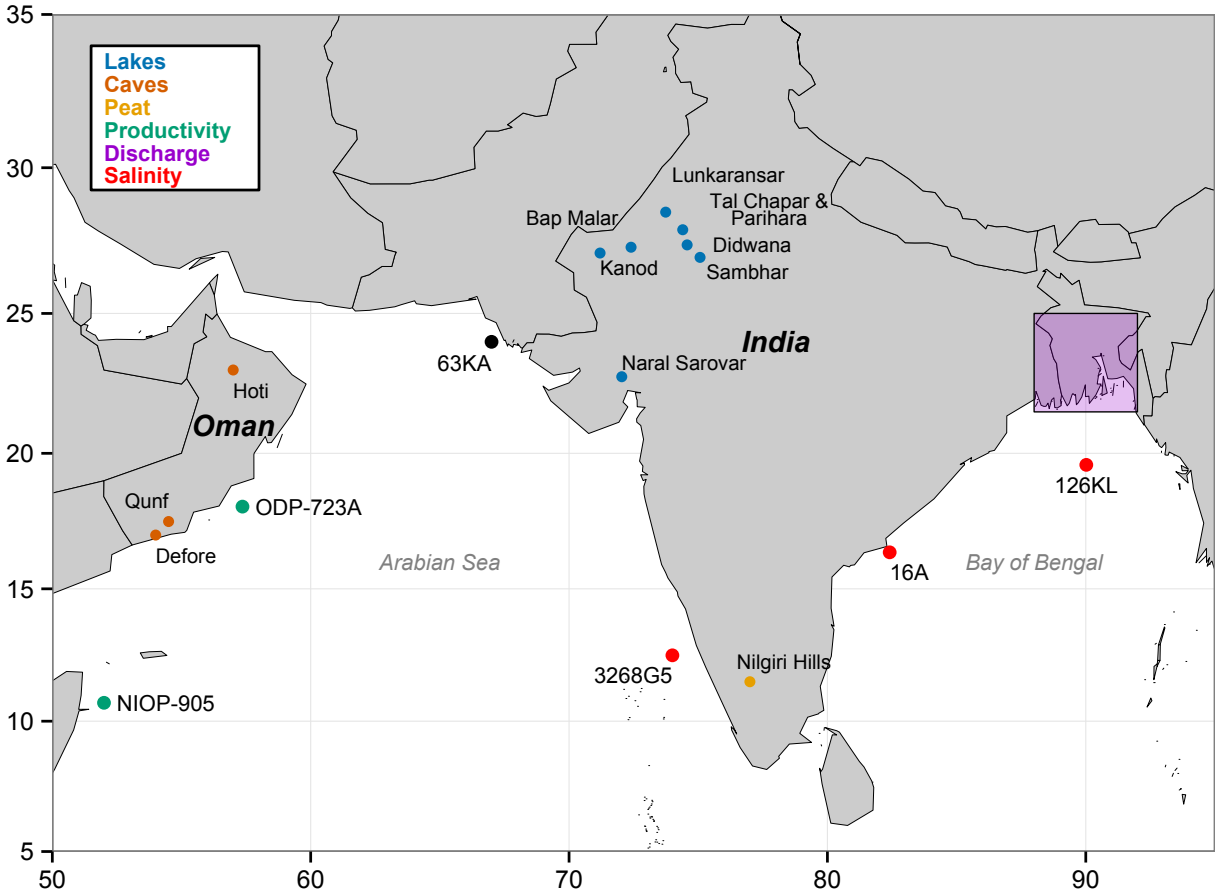

Figure 1. A partial summary of the locations of different types of proxy records that have been reconstructed through the past 10 ka, and suggest enhanced wetness over India during the early- to mid-Holocene and aridification during the late Holocene. This figure and the original studies citing each proxy is discussed in further detail in the Section 2: Paleoclimatic Evidence of a Wetter India.

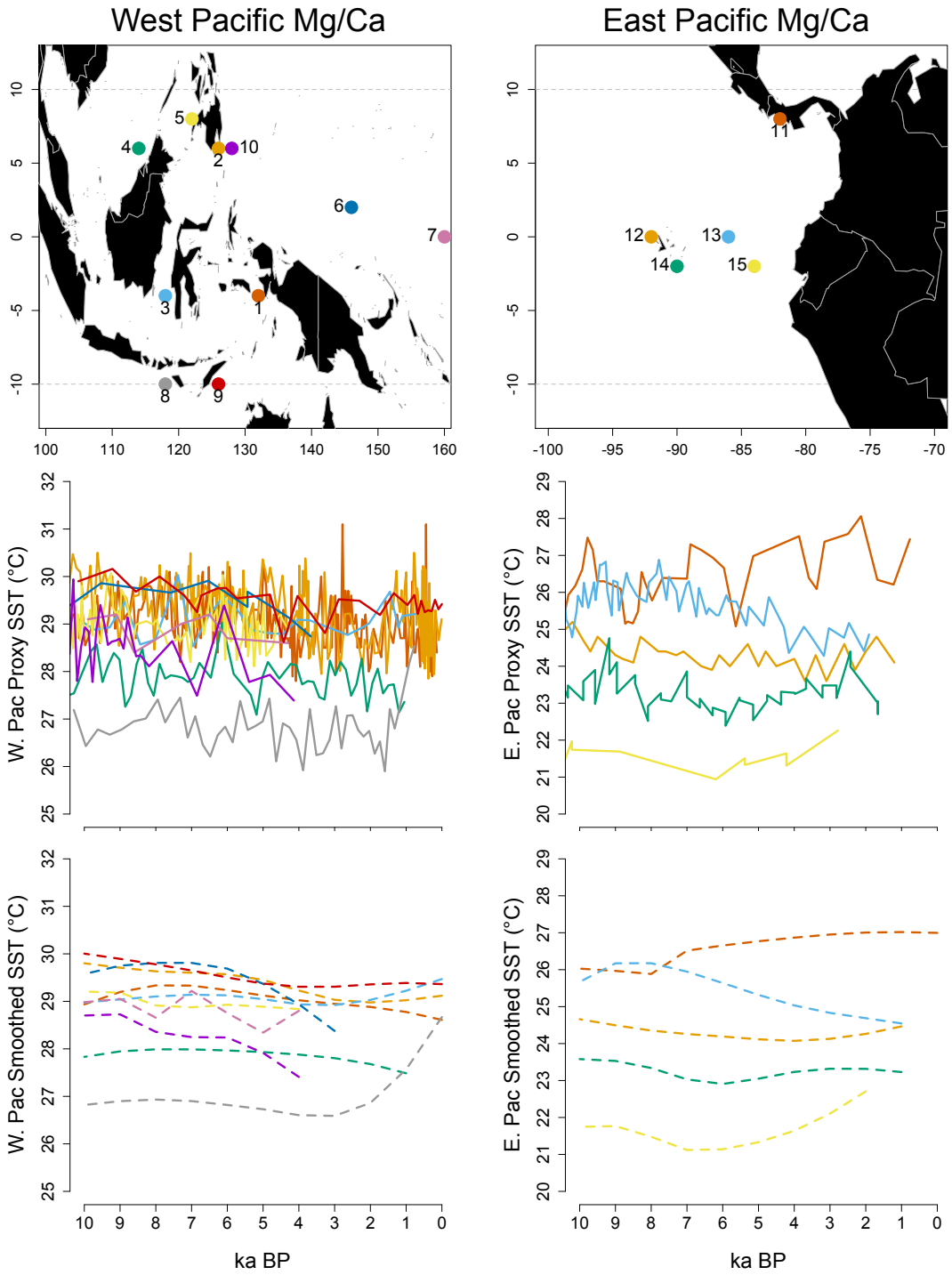

Figure 2. Maps of eastern and western equatorial Pacific Ocean Mg/Ca SST records. The second row provides raw SST estimations as calibrated by original authors listed in Table 1. The third row provides the records smoothed by a second order local polynomial method with a local neighborhood of 70% nearest data points.

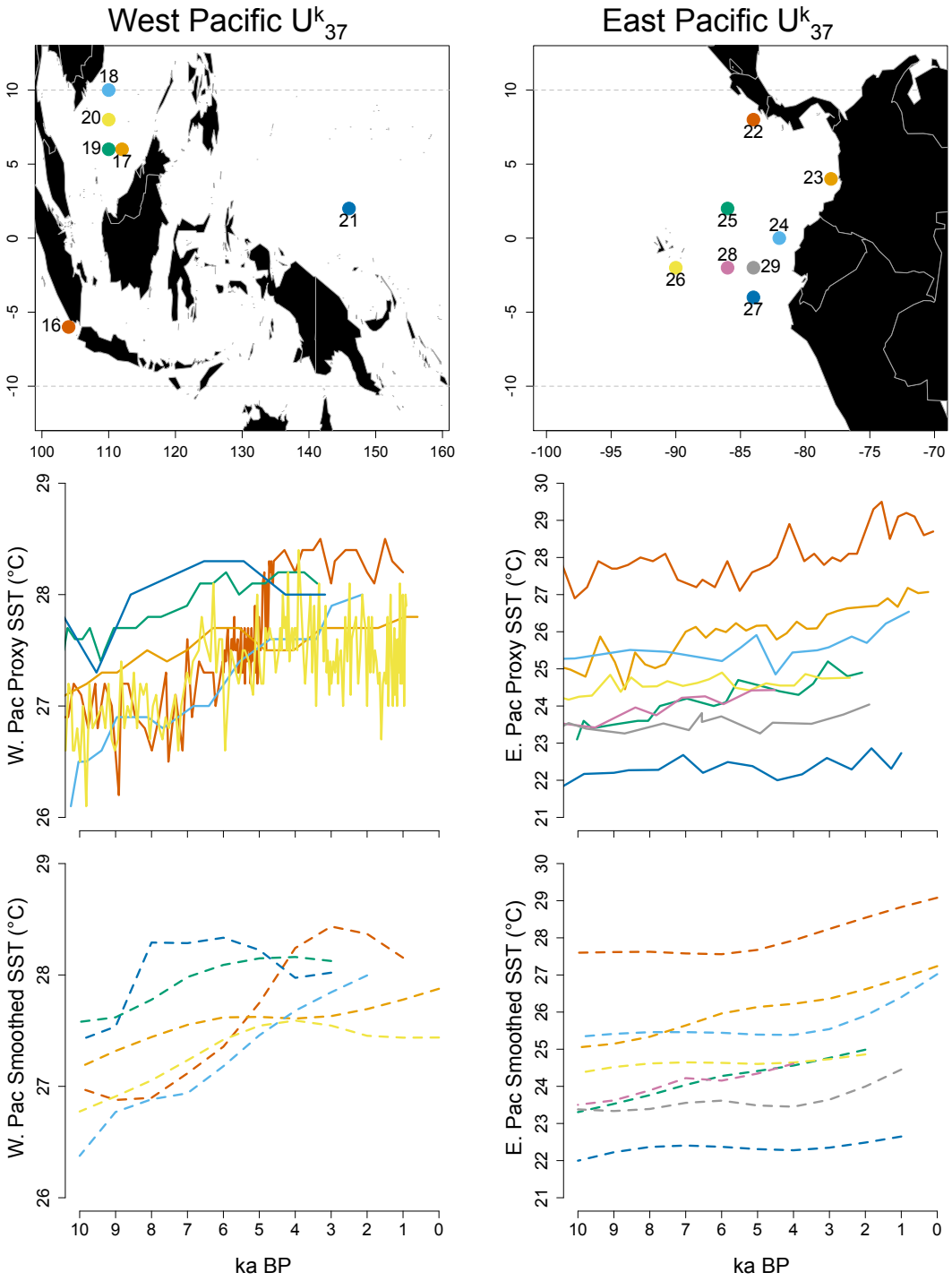

Figure 3. Same as Figure 2, but for $U^{k'}_{37}$ proxy records. Authors of these records are listed in Table 2.

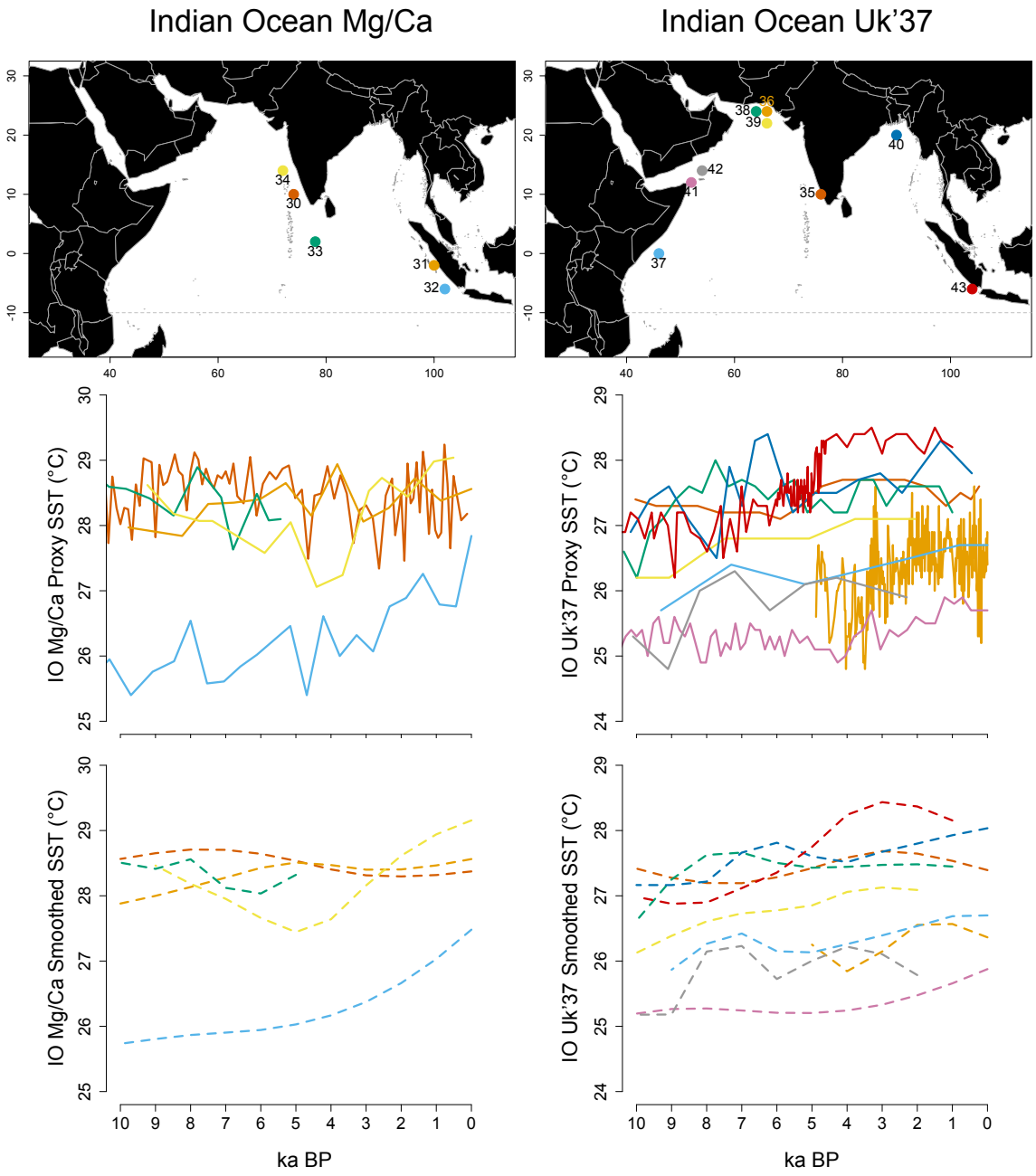

Figure 4. Maps of Indian Ocean Mg/Ca and $U^{k'}_{37}$ SST records. The second row provides raw SST estimations as calibrated by original authors listed in Table 3. The third row provides the records smoothed by a second order local polynomial method with a local neighborhood of 70% nearest data points.

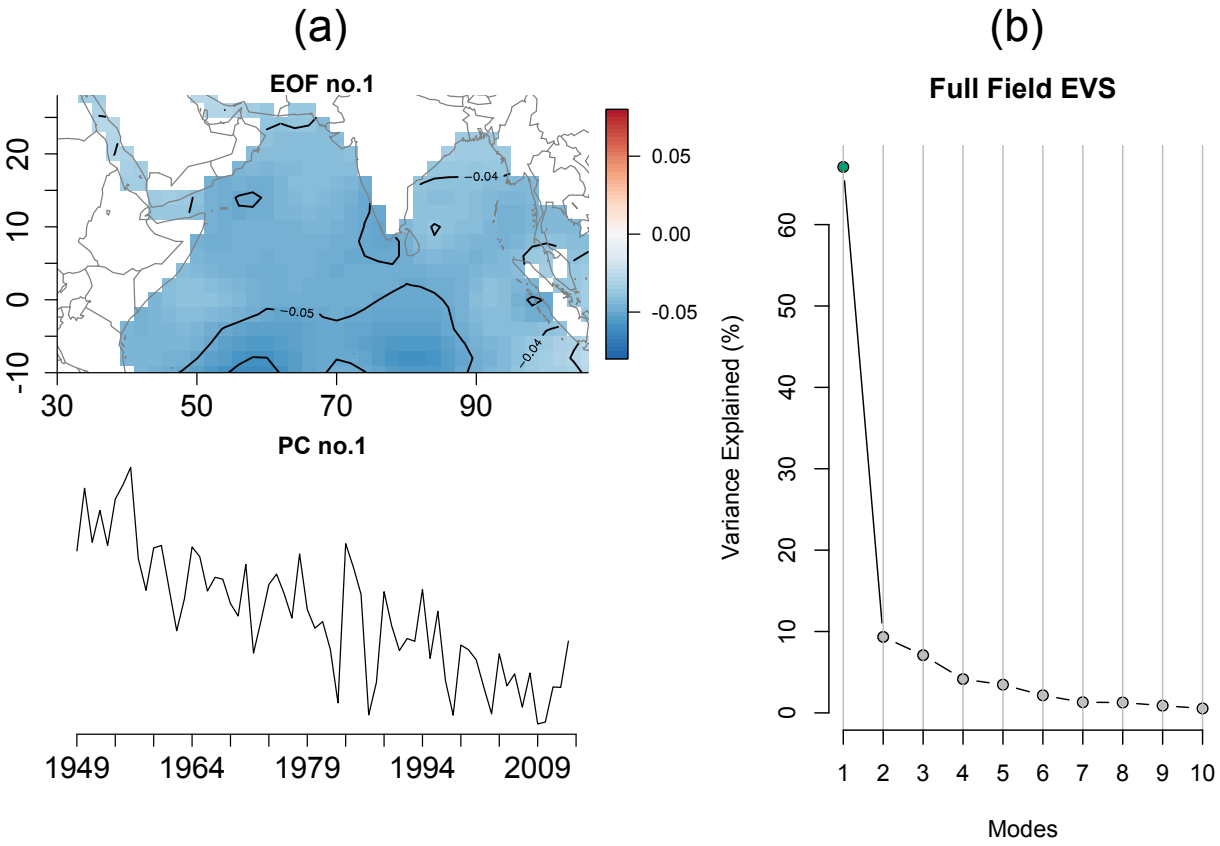

Figure 5. First orthogonal mode of summer (June-Sep) Indian Ocean SSTs from 1949-2013 [*Smith et al.*, 2008]. As shown by the spatial EOF (a, top) and the PC (a, bottom), the most dominant mode is a strong contemporary trend. The influence of this trend was removed from summer contemporary wind data prior to paleo-reconstructions. This mode accounts for nearly 70% of the total variance of the data, which can be seen on the eigenvalue spectrum (right, b), which explains the resolved variance of each of the first ten modes. The 2^{nd} and 3^{rd} modes explain 9% and 7% of the total variance, respectively. The 4^{th} mode, and all modes after, each explain less than 5% of the total variance.

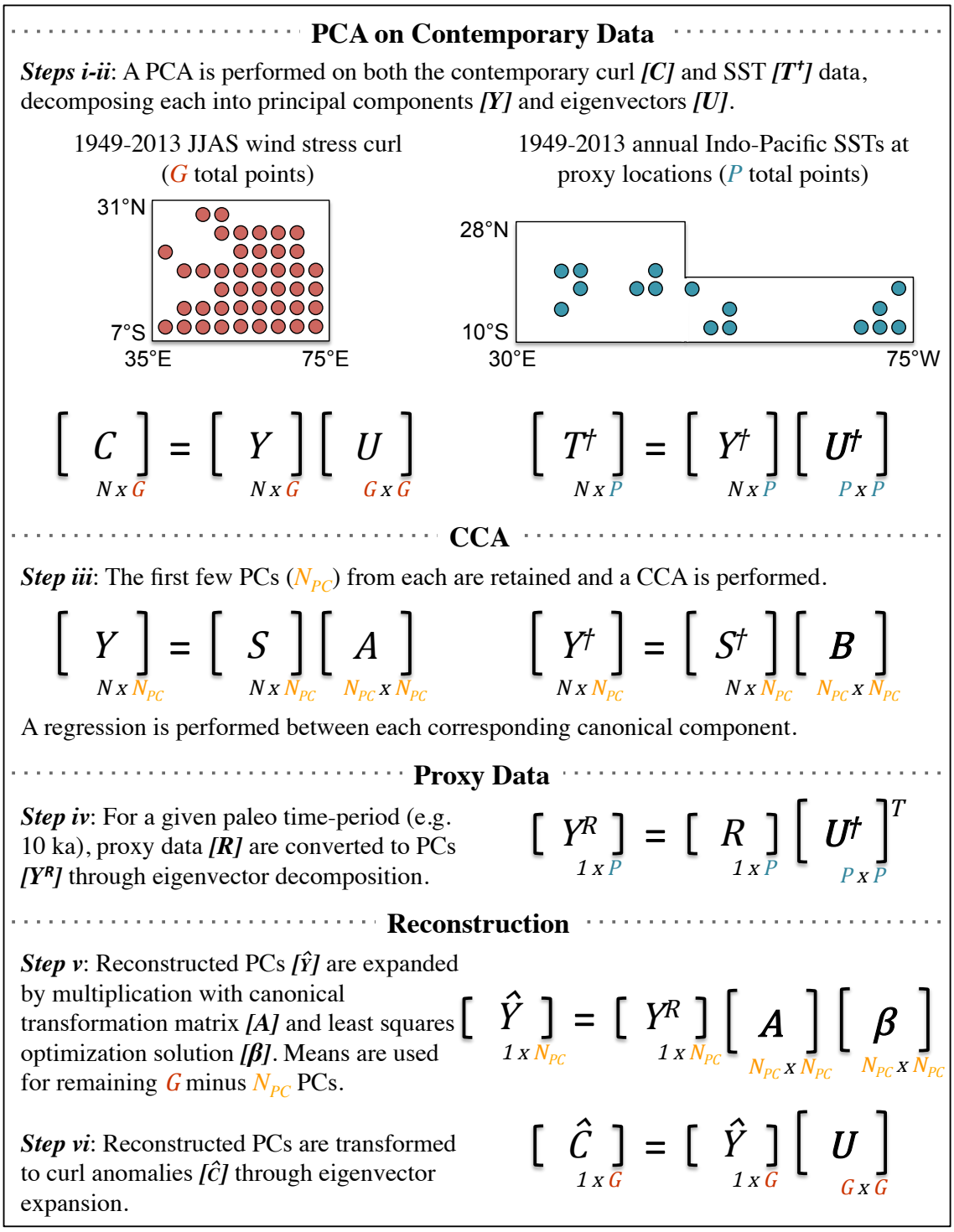

Figure 6. A diagram of the main steps of the CCA reconstruction methodology. The steps are given for producing SSTs representative of 10 ka. *Steps (iii-vi)* are repeated for 8, 6, 4, and 2 ka.

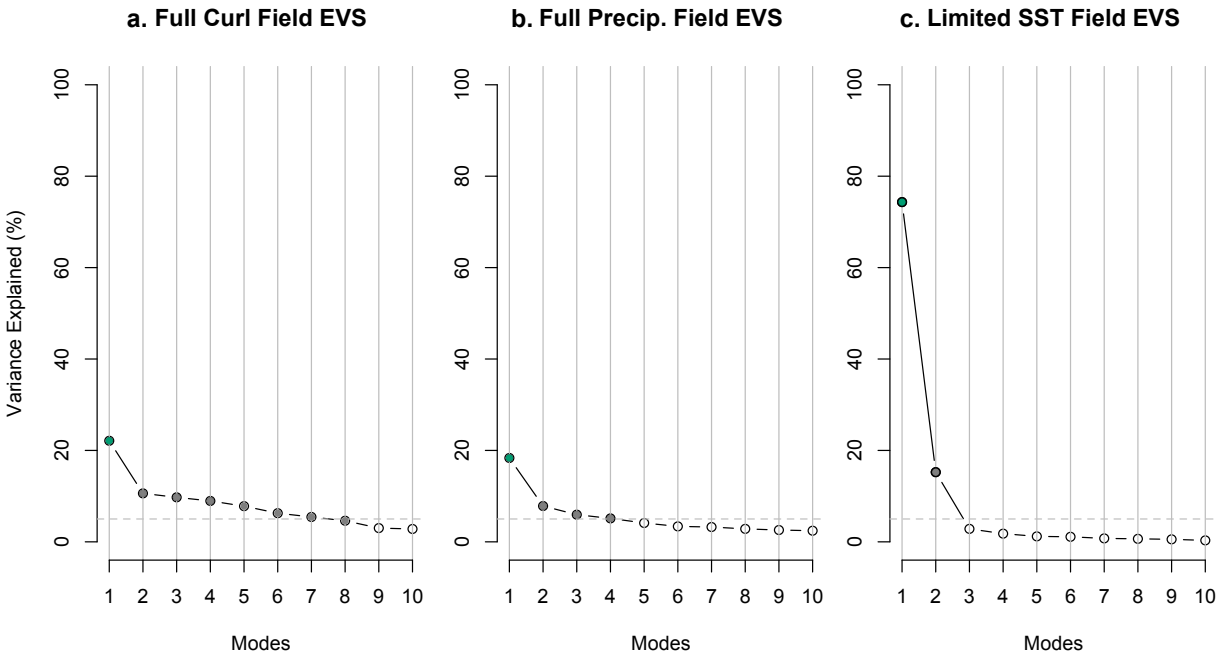

Figure 7. Eigenvalue spectrums (EVS) for the (a) full field of Arabian Sea summer wind stress curl (1949-2013) [*Kalnay et al.*, 1996], (b) full field of Indian summer monsoon rainfall (1901-2004) [*Rajeevan et al.*, 2006], and (c) limited Indo-Pacific SST field (1949-2013) [*Smith et al.*, 2008]. The green points represent the variance explained by the first mode of each field. The grey dots represent all subsequent modes that each explain at least 5% of the total variance of the respective datasets. This 5% threshold was considered in deciding how many PCs to retain for each CCA reconstruction.

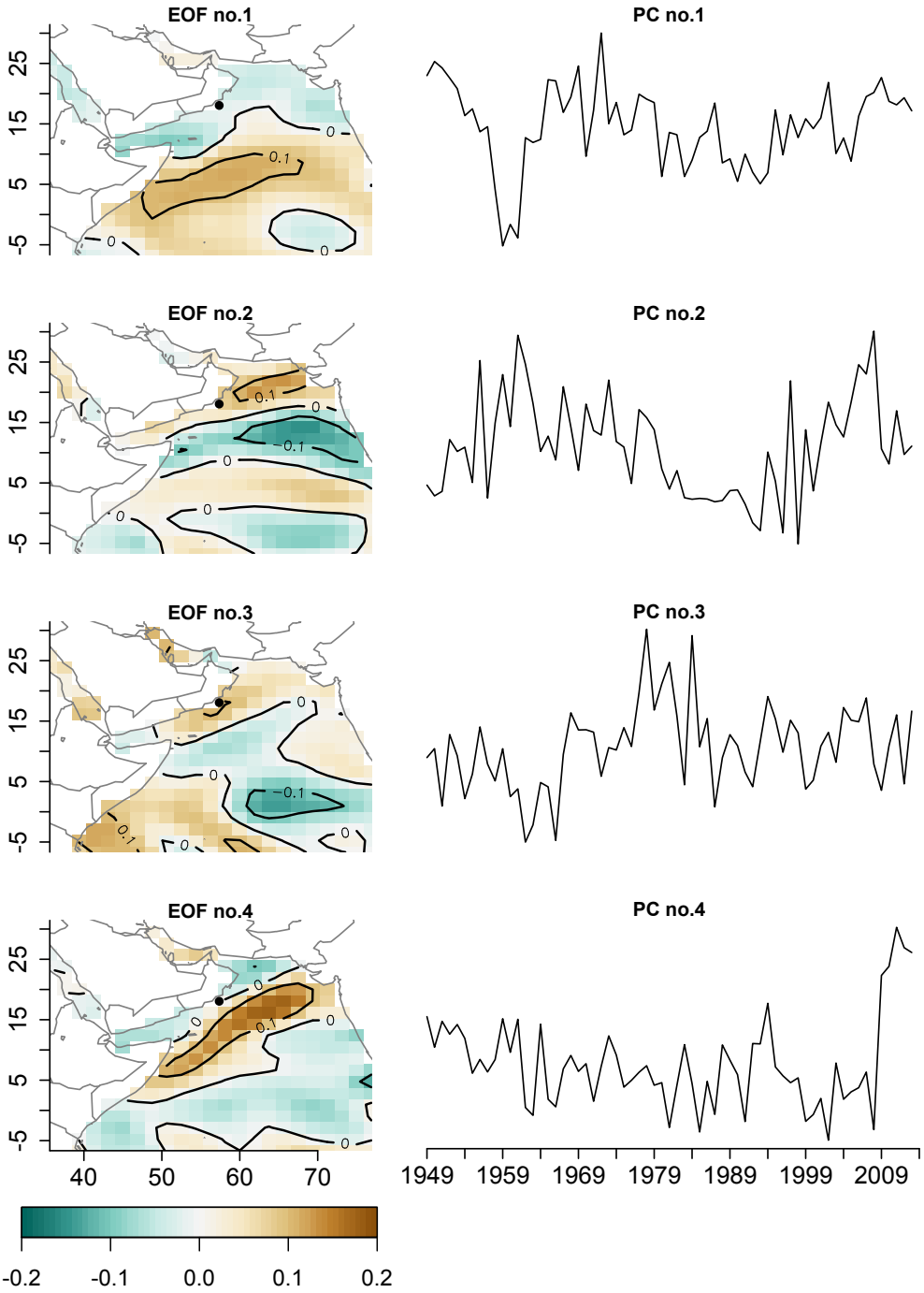

Figure 8. First four orthogonal EOFs and PCs of Arabian Sea summer wind stress curl over the monsoon region from 1949-2013 [*Kalnay et al.*, 1996]. The first four modes of wind stress curl explain 22.1%, 10.6%, 9.7%, and 8.9%, respectively, of the full field variance. The black point off the coast of Oman indicates the location of the *Gupta et al.* [2003] *G. bulloides* record.

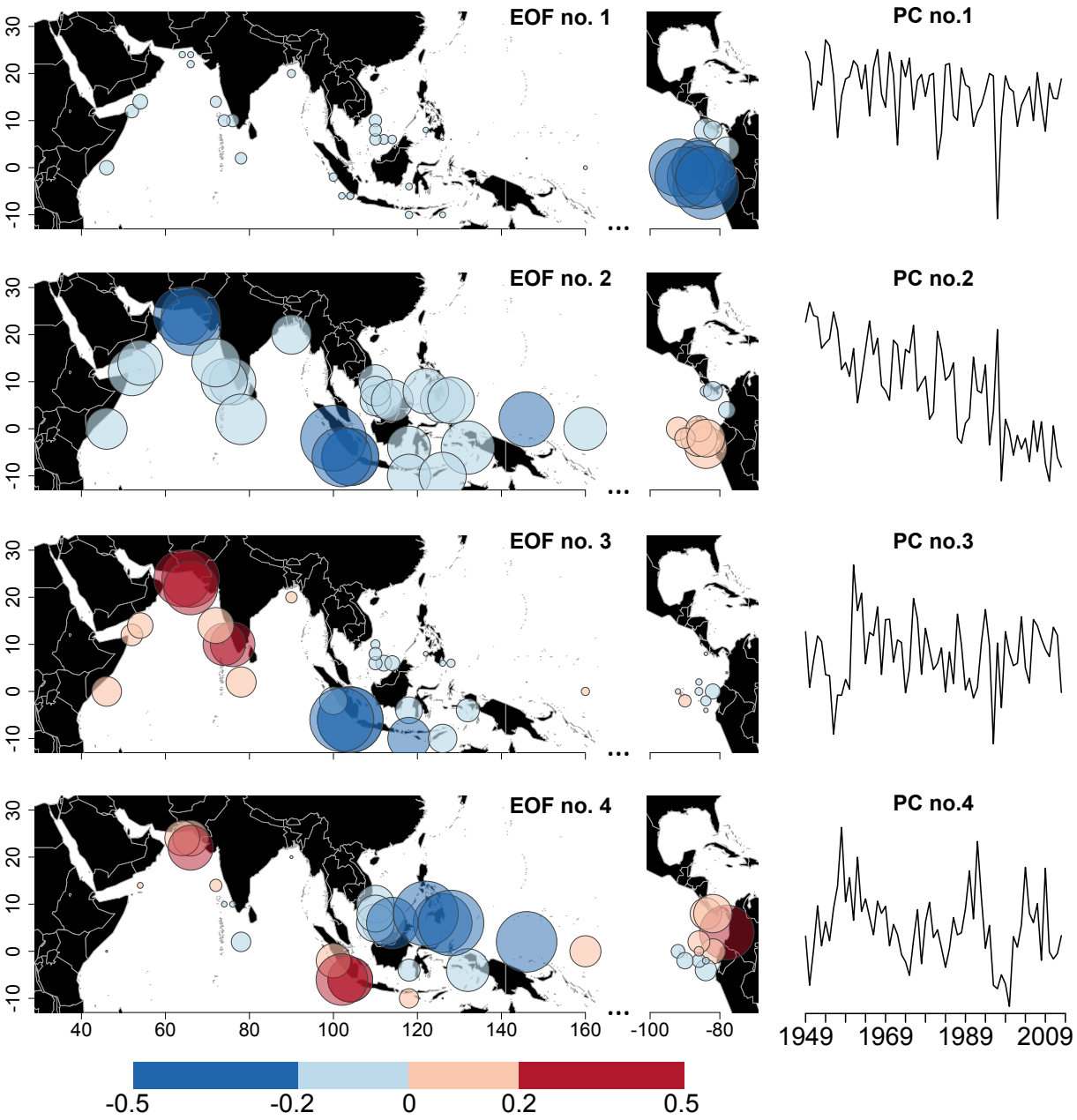

Figure 9. First four EOFs of the limited SST field using data from *Smith et al.* [2008]. The first four modes of the limited Indo-Pacific SST field account for 74.3%, 15.2%, 2.8%, and 1.8% of the limited field variance.

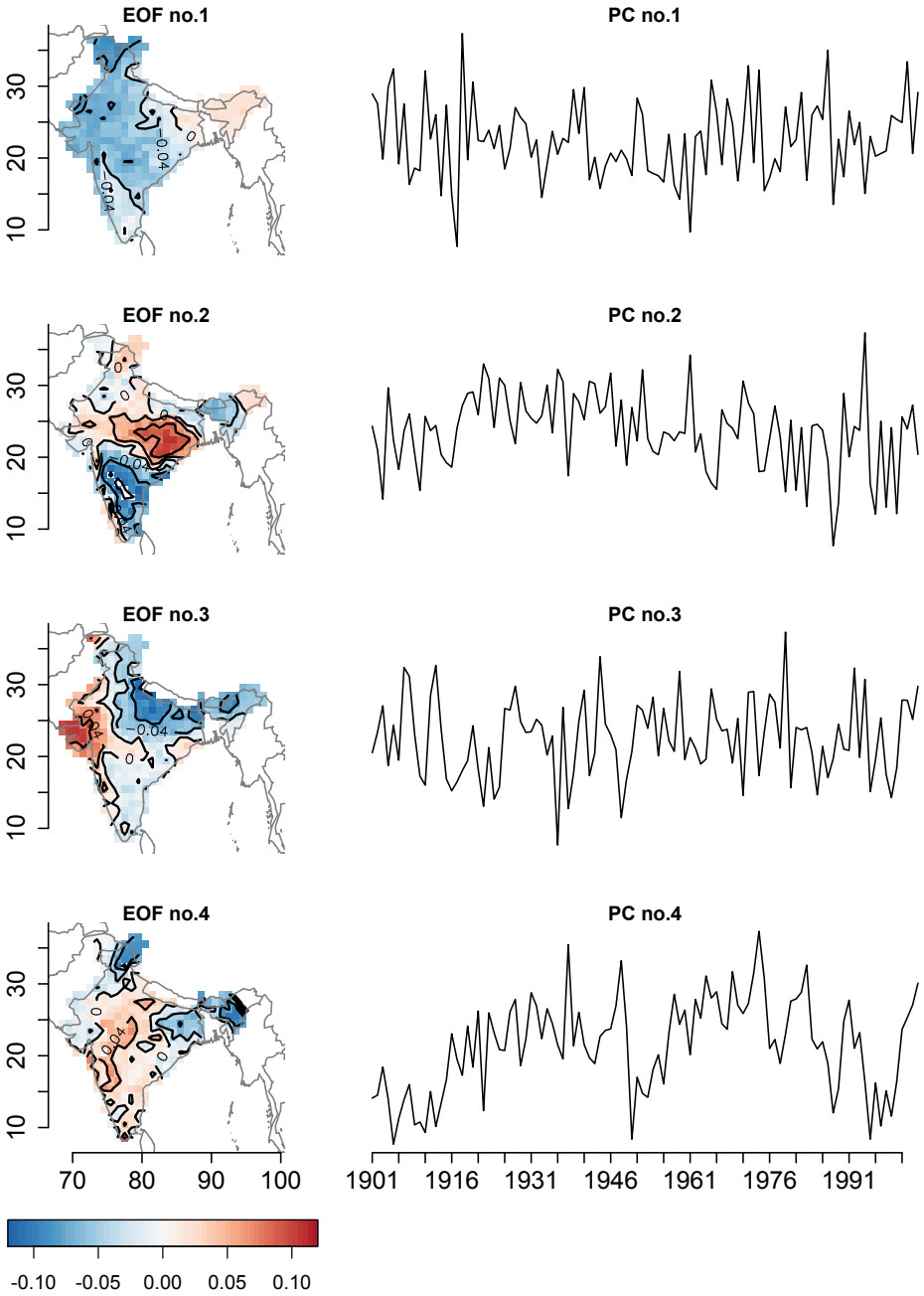

Figure 10. First four EOFs of the Indian summer monsoon rainfall field using data from *Rajeevan et al.* [2006]. The first four modes account for 18.3%, 7.8%, 5.9%, and 5.1% of the full field variance.

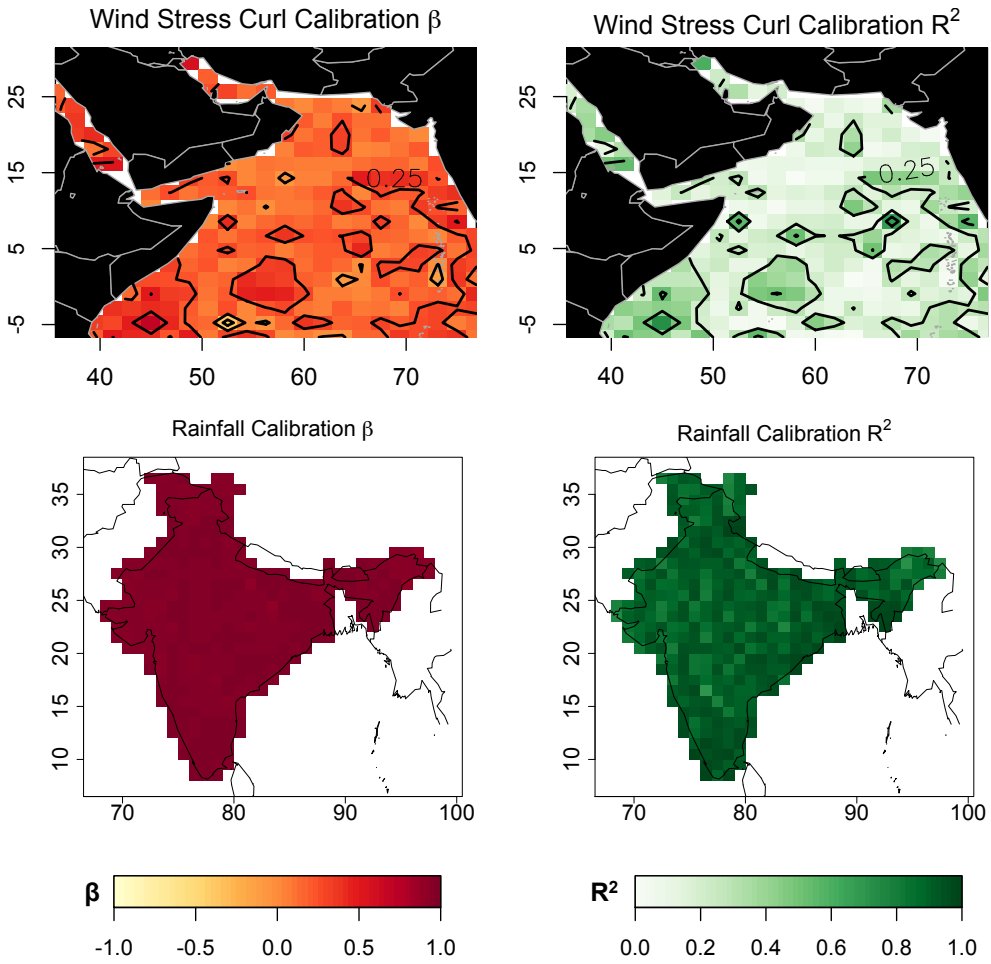

Figure 11. Model calibration statistics for wind stress curl (top; using the first 8 PCs), and rain (bottom; using the first 4 PCs) for the CCA-based reconstruction models. The β-statistic (left) represents the resolved variance captured by the reconstructed contemporary data (1949-2013 for wind stress curl, 1901-2004 for rain). The R^2 (right) provides the correlation between the observed contemporary data and the reconstructed contemporary data. These statistics are calculated on the PC signal only, which is further clarified in the text.

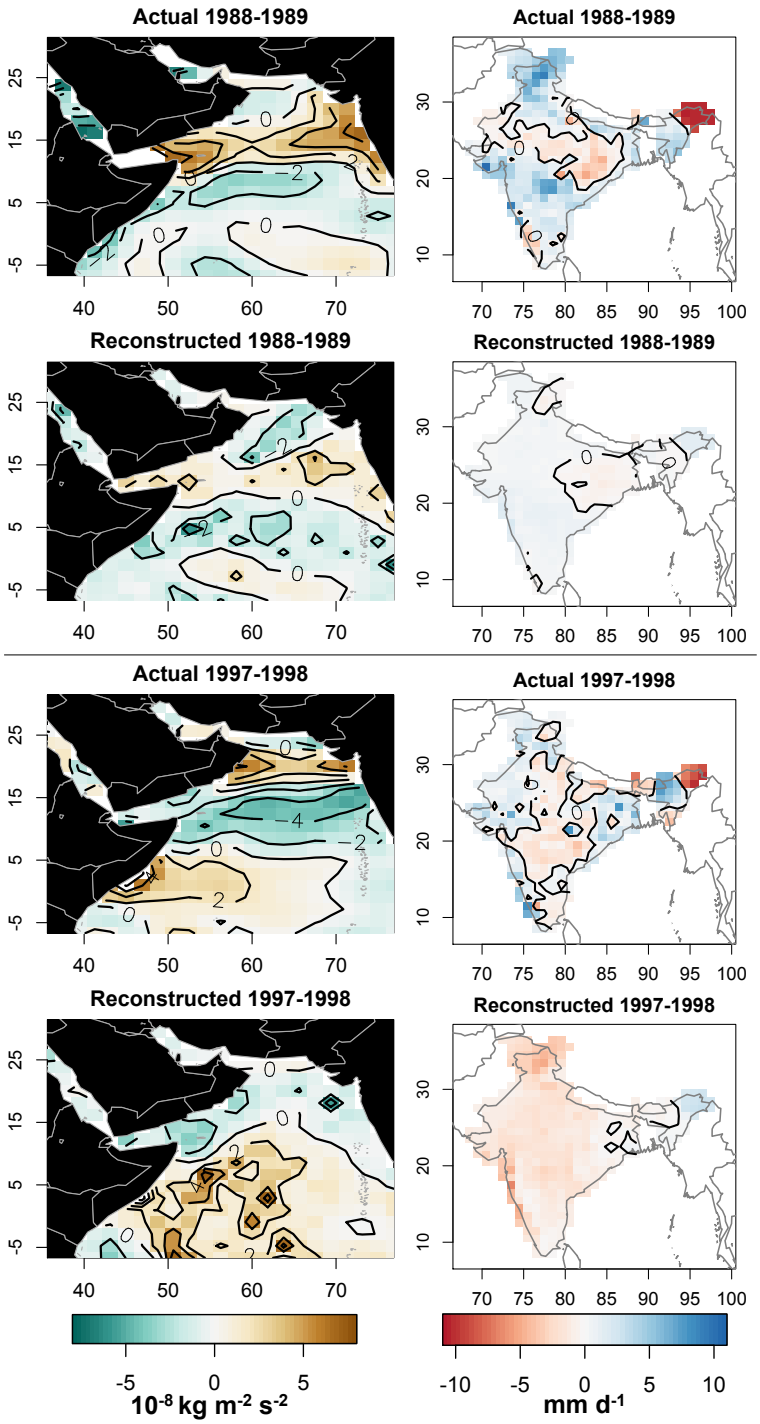

Figure 12. Actual and reconstructed wind stress curl (10^{-8} kg m^{-2} s^{-2}) and rain anomalies ($mm\ d^{-1}$) for 1988-1989 (a strong La Nia year and strong monsoon year) and 1997-1998 (a strong El Nio year and weak monsoon year). Contour lines on rainfall plots indicate zero.

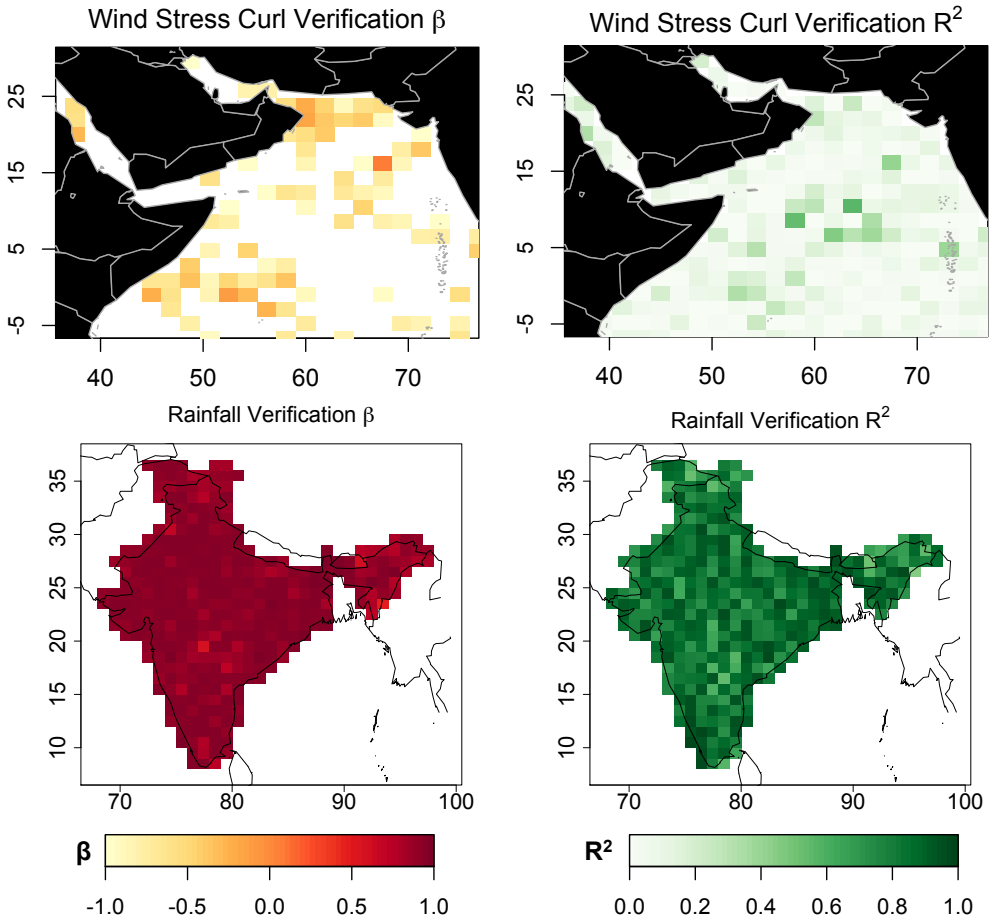

Figure 13. Model verification performed by training the model on the most recent period (1980-2013 for wind stress curl, 1980-2004 for rainfall), and using that model to validate the period prior (1949-1979 for winds and 1901-1979 for rain). The β- and R^2-statistics are used once again to quantify model skill and the statistics are calculated in the PC signal only.

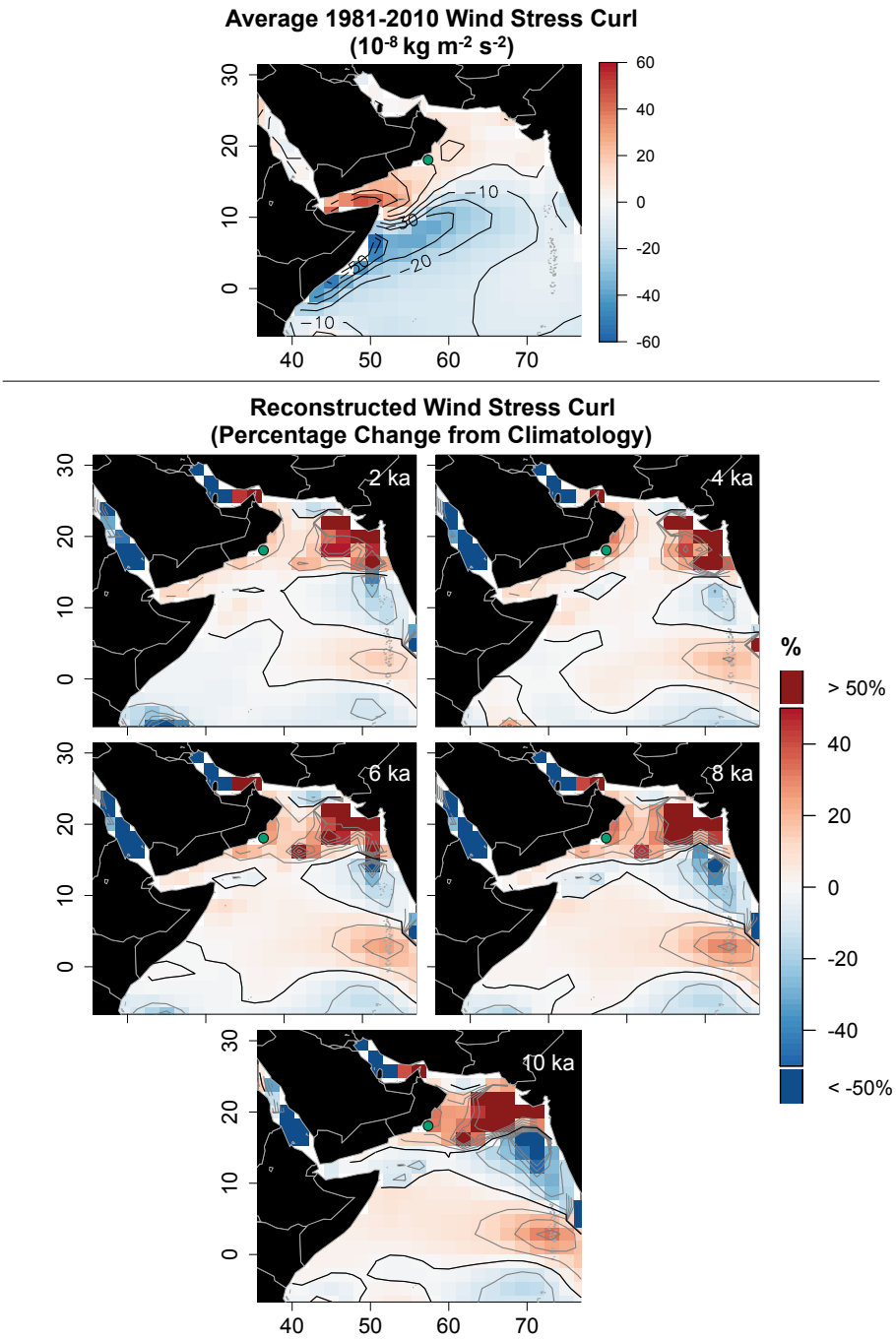

Figure 14. Multi-proxy reconstructed summer wind stress curl anomalies for 10, 8, 6, 4, and 2 ka over the Arabian Sea region. Reconstructions are presented as percentage departures from the present day mean. The green point off the coast of Oman in the northwestern Arabian Sea indicates the location of the *G. bulloides* productivity/upwelling reconstruction provided by *Gupta et al.* [2003]. The present day 1981-2010 climatology is presented at the top of the figure.

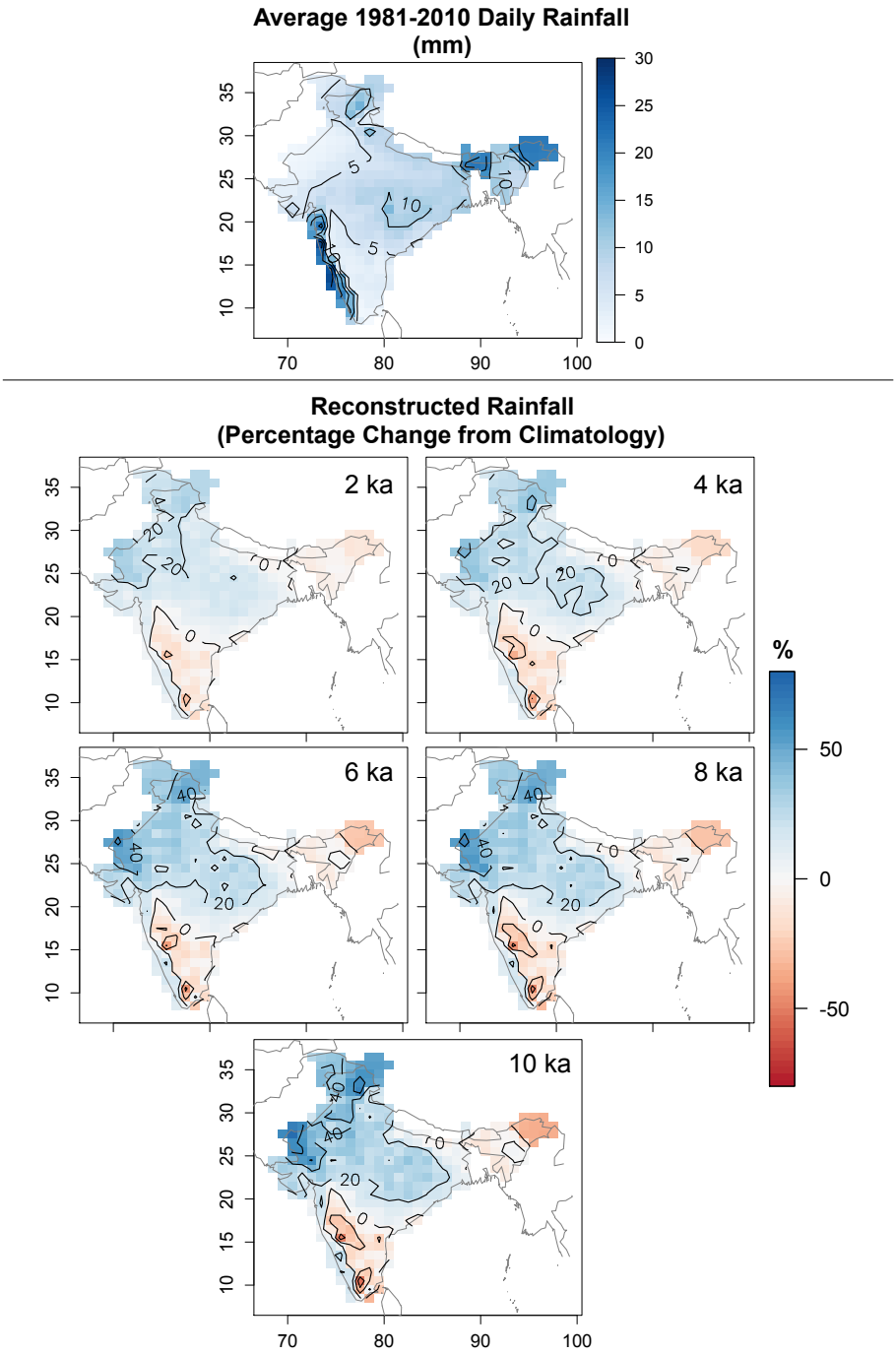

Figure 15. This is the same as Figure 15, but for the multi-proxy reconstructed summer monsoon rainfall over India.

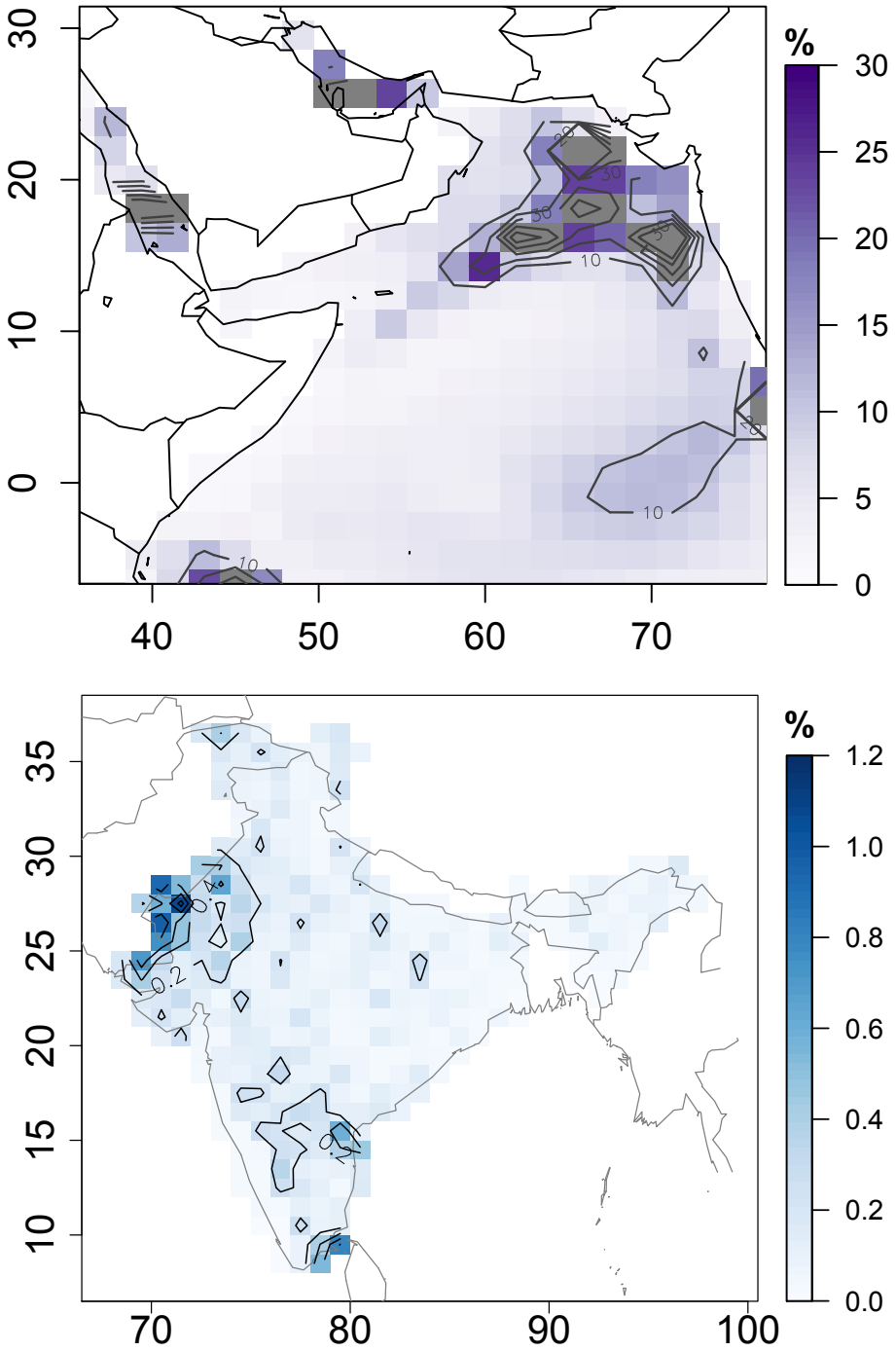

Figure 16. Standard error calculated from the actual 1949-2013 wind stress curl and 1901-2004 rain anomalies and those reconstructed by the limited proxy field. Grey indicates values greater than 30%.

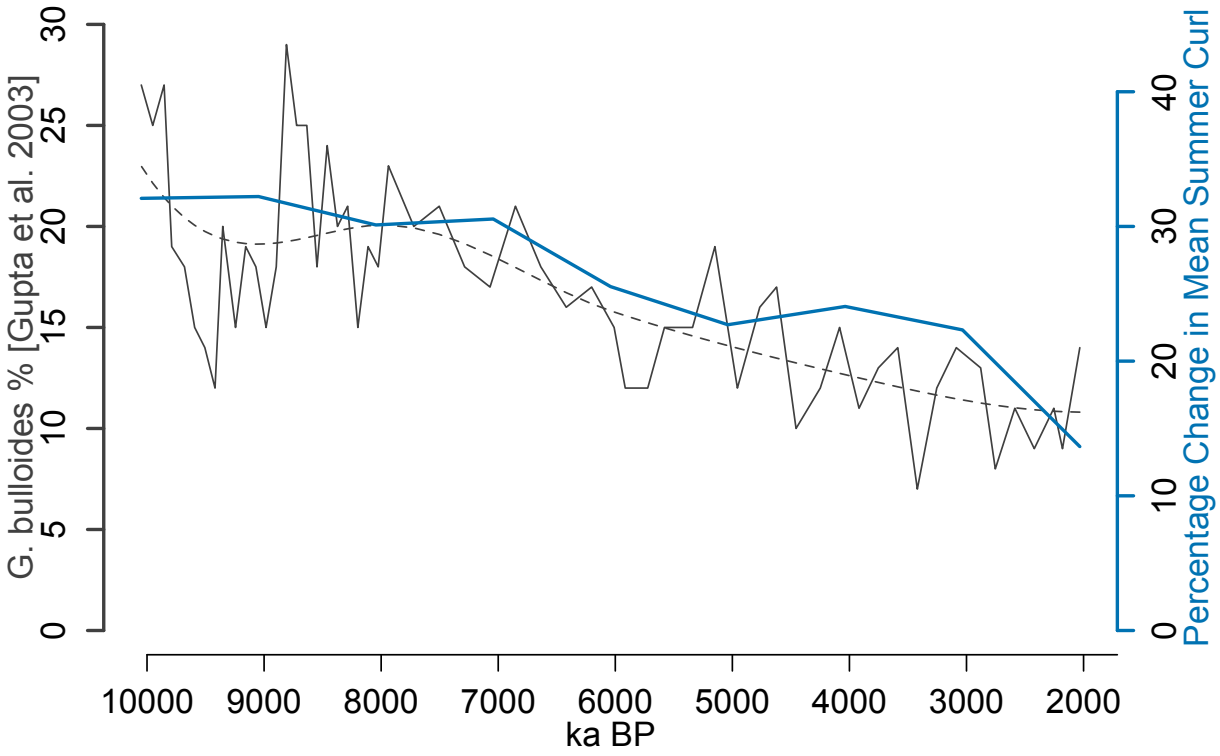

Figure 17. Comparison of the *Gupta et al.* [2003] *G. bulloides* reconstruction of (black) to reconstructed percentage change in wind stress curl (blue) from 10 to 1 ka. A local polynomial is used to smooth the *G. bulloides* data and is provided by the dotted line.

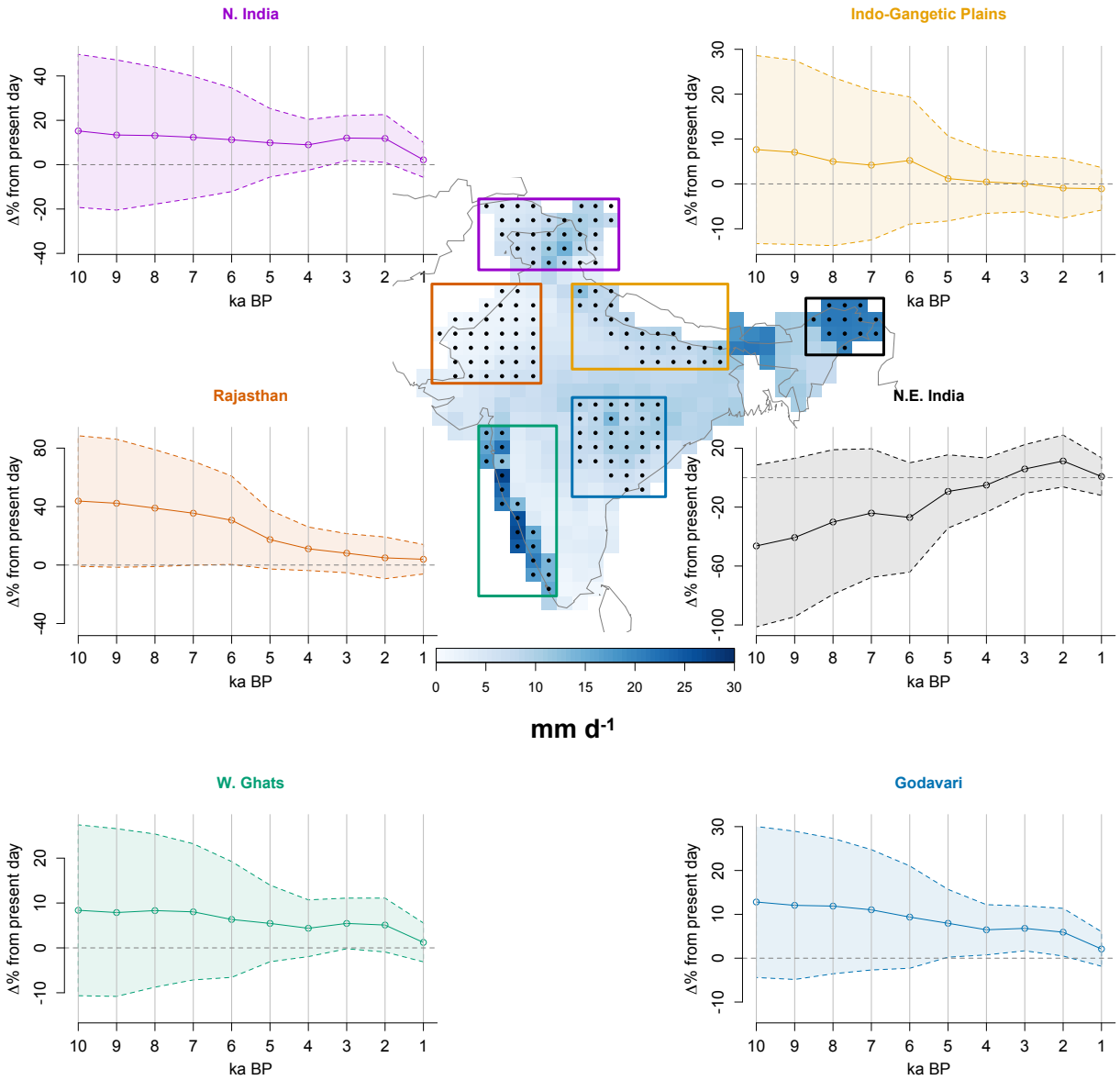

Figure 18. Reconstructed mean daily rainfall ($mm\ d^{-1}$) for the monsoon season for six regions: (a) Northern India, (b) Rajasthan, (c) Western Ghats (green), (d) Indo-Gangetic Plains, (e) North East India, and (f) Godavari River Basin. The stippled regions inside the larger boundaries are the grid cells used for each respective reconstruction. *Rajeevan et al.* [2006] mean daily rainfall from 1901-2004 is shaded on the map. Rainfall is reconstructed by mean daily monsoon rainfall from each stippled region as a function of the limited field SST proxies.